Article

Protonated Organic Diamines as Templates for Layered and Microporous Structures: Synthesis, Crystal Chemistry, and Structural Trends among the Compounds Formed in Aqueous Systems Transition Metal Halide or Nitrate–Selenious Acid

Dmitri O. Charkin [1], Evgeny V. Nazarchuk [2], Dmitri N. Dmitriev [1], Vasili Yu. Grishaev [2], Timofey A. Omelchenko [1], Darya V. Spiridonova [3] and Oleg I. Siidra [2,4,*]

[1] Inorganic Chemistry Division, Chemistry Department, Moscow State University, Vorobievy Gory, 1-3, 199991 Moscow, Russia; d.o.charkin@gmail.com (D.O.C.); ddn063@gmail.com (D.N.D.); tomelchenko003@gmail.com (T.A.O.)

[2] Department of Crystallography, Institute of Earth Sciences, St. Petersburg State University, 199034 St. Petersburg, Russia; e_nazarchuk@mail.ru (E.V.N.); grishaevv98@mail.ru (V.Y.G.)

[3] X-ray Diffraction Resource Center, St. Petersburg State University, 199034 St. Petersburg, Russia; daria.spiridonova@spbu.ru

[4] Kola Science Center, Russian Academy of Sciences, Fersman Str. 14, 184209 Apatity, Russia

[*] Correspondence: o.siidra@spbu.ru

Abstract: Systematic studies of crystalline compounds formed in aqueous systems containing aliphatic diamines, divalent transition metal halides, and selenious acid resulted in the discovery of a large family of new complex species corresponding to several new structure types. With ethylenediamine (en), layered $(enH_2)[M(HSeO_3)_2X_2]$ compounds are the most commonly formed species which constitute a significant contribution to the family of layered hydrogen selenites containing neutral $[M(HSeO_3)_2]$ (M = Mg, Mn, Co, Ni, Cu, Zn, Cd) $2D$ building blocks. In contrast to some previous suggestions, piperazine (pip), as well as its homologue N-methylpiperazine, mostly give rise to quite different, sometimes more complex, structures of varied dimensionality while the $(pipH_2)[M(HSeO_3)_2X_2]$ compounds are formed only with M = Cu and Cd. In addition, metal-, halide-, or selenium-free by-product species are observed. The Se^{IV} can be present in a multitude of forms, including H_2SeO_3, $HSeO_3^-$, SeO_3^{2-}, and $Se_2O_5^{2-}$, reflecting amazing adaptability to the shape of the templating cations.

Keywords: selenites; transition metals; metal halides; organically templated compounds; synthesis; microporous structures; protonated organics

1. Introduction

The use of "lone-pair" cations and halide or nitrate anions is well known to lead to numerous open-framework, porous, and non-centrosymmetric structures [1–5]; addition of magnetically active cations of *d*- and *f*-elements frequently gives rise to unusual architectures and magnetic responses. Yet, most attention is dedicated to fully deprotonated acid residues, e.g., selenites, tellurites, or iodates, while the acid salts and other hydrogen-bonded networks have as yet received less attention, although at least some of these species exhibit several attractive properties [6–8].

A numerous yet sparsely addressed family of mostly inorganic compounds is formed by the "layered hydroselenites", first described by Trombe et al. [9–11] and further extended in our studies [12–15] among compounds of copper. Later, some zinc [16], cobalt

[17–20], and cadmium [21] containing species were reported. The crystal chemistry of this family is relatively diverse and the overwhelming majority of structure types and their representatives are the copper compounds. The structures of these compounds contain quasi-planar $[M^{II}(HSeO_3)_2]^0$ layers formed by Cu^{2+} cations and hydrogen-bonded dimers of $HSeO_3^-$ anions forming a distorted quasi-square grid. The interlayer space can be either empty, as in $Cu(HSeO_3)_2$ [22], filled with water molecules, as in $Cu(HSeO_3)_2 \cdot 2H_2O$ [9], various metal-halide [11–13,15–17,20] and metal-nitrate [14] slabs, or more complex species such as $[M^{II}(H_2O)_4][Cu(HSeO_3)_2Cl_2]$ series (M^{II} = Mn–Zn, Fe excepted) [10,18] and $[Co(H_2O)_4][Co(HSeO_3)_2Cl_2]$ [20]. It is noteworthy that the bromide analogs of the two latter compounds, as well as alkali–cobalt selenite chlorides [17], have not been reported, while within the $(A^IX)[Cu(HSeO_3)_2]$ series (A^I = Na, K, Rb, Cs, NH$_4$) [13], as well as $(RbX)[Zn(HSeO_3)_2]$ [16], bromides are full structural analogs of the corresponding chlorides. Several nitrate-containing copper compounds are also known [9,16].

Among halides, ammonium compounds are complete structural analogs of the rubidium- and cesium-containing species [13,16], while among nitrates, they contribute to the compound with the most complex interlayer architecture, $(NH_4NO_3)_3[Cu(HSeO_3)_2]$ [9], which was tentatively attributed to the ability of the NH_4^+ cations to form strong directional hydrogen bonds to the nitrate anions. This suggests that some other species, particularly organic ammonium cations, may also be incorporated into the interlayer space. This was initially demonstrated by the preparation of cadmium-containing compound $(enH_2)[Cd(HSeO_3)_2Cl_2]$ (enH_2^{2+} = ethylenediammonium cation, $H_3NCH_2CH_2NH_3^{2+}$) [21]; later, isostructural cobalt and copper-based compounds were reported [19]. The layer topology in their structure is essentially the same as that in $[M(H_2O)_4][Cu(HSeO_3)_2Cl_2]$, $[Co(H_2O)_4][Co(HSeO_3)_2Cl_2]$, and $[A_2(H_2O)_n][Co(HSeO_3)_2Cl_2]$ (A = K, n = 2; A = Cs, n = 0). The existence of a related piperazinium compound was also noted in [21]; however, no data have been reported nor possible analogs mentioned. Yet, ethylenediammonium and piperazinium cations are characterized by nearly the same distances between the ammonium hydrogen bond donor centers, though the number of "active" N–H bonds is different (6 vs. 4). In the current study, we performed an extensive search for possible analogs among hydrogen selenite–halides of diprotonated ethylenediamine (enH_2^{2+}), piperazine ($pipH_2^{2+}$), N,N'-dimethlethylenediamine ($dmedaH_2^{2+}$), and N-methylpiperazine ($mpipH_2^{2+}$) species (Figure 1) and transition metals reported earlier to form the $[M^{II}(HSeO_3)_2]$ slabs, namely Co, Cu, Zn, and Cd. In addition, test experiments were also performed with magnesium, manganese, and nickel halides.
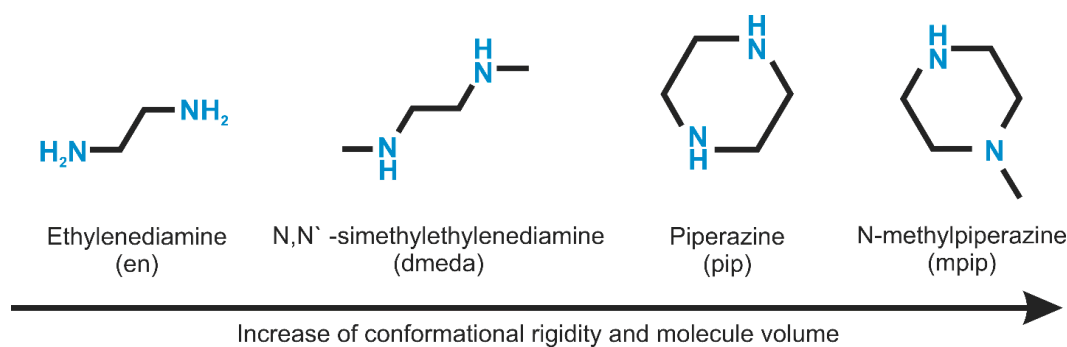

Figure 1. Organic templates used in the current study.

The outcomes of the solution syntheses depended mostly on the nature of the organic species used. The majority of the new species belong to the targeted hydroselenite family; however, representatives of other, more compositionally simple families were also observed. These can be roughly collected into the following groups: (i) the "layered hydroselenites" containing all elements involved; (ii) framework selenite–diselenites with no incorporated halide or nitrate; (iii) ion-molecular crystals of ethylenediammonium salts and selenious acid which do not contain the divalent metal; and (iv) halometallates

of organic cations which do not incorporate selenium.

2. Results and Discussion

2.1. (enH$_2$)[M(HSeO$_3$)$_2$X$_2$] (X = Cl and Br)

Representatives of this structure type have been found among compounds of Co, Cu, Zn, and Cd, that is, for all M^{2+} cations where the formation of [M(HSeO$_3$)$_2$] layers had been reported (vide supra); the new contributors to this series are Mn^{2+}, Ni^{2+}, and probably Mg^{2+} (Table 1). Similar to (AX)[M(HSeO$_3$)$_2$] (M = Cu, Zn) and in contrast to [M'(H$_2$O)$_4$][M(HSeO$_3$)$_2$], both chlorides and bromides were found to exist. Bromides have not been observed yet for Mg^{2+} and Ni^{2+}; most likely these compounds exist but are less stable and more sensitive to the preparation conditions. Numerous attempts to prepare acceptable quality crystals for the elusive (enH$_2$)[Mg(HSeO$_3$)$_2$Cl$_2$] have not been successful; the cell metrics and positions of non-hydrogen atoms correspond to the same arrangement.

In the structures of (enH$_2$)[M(HSeO$_3$)$_2$X$_2$] (M = Cd, Co, Cu, Mn, Zn; X = Cl, Br), the metal cations center slightly distorted *trans-MO$_4$X$_2$* octahedra (Figure 2). The bond valence sums on M^{2+} cites agree well with the oxidation state of 2. The distortion indices for the octahedra (Table 2) were calculated using the Vesta suite [23].
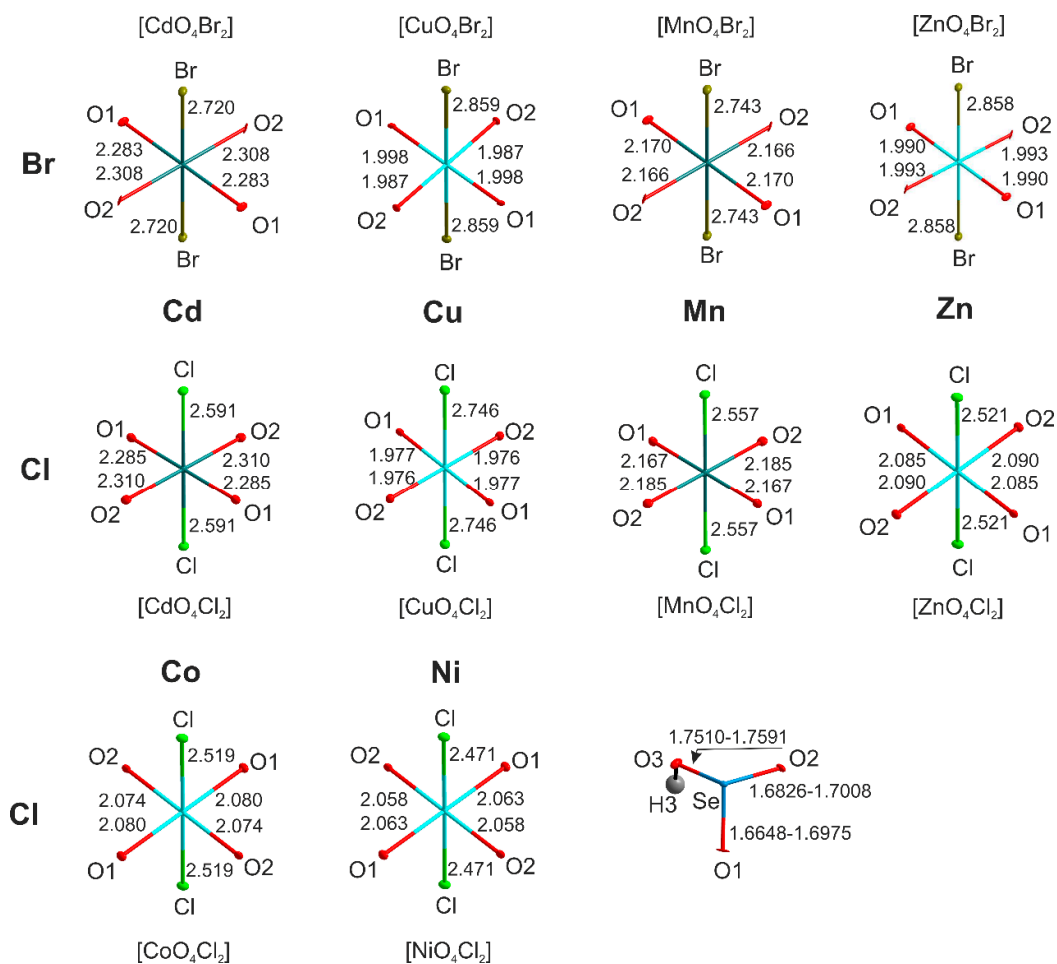

Figure 2. Cation coordination in (enH$_2$)[M(HSeO$_3$)$_2$X$_2$].

Table 1. Crystallographic and refinement parameters for $(enH_2)[M(HSeO_3)_2X_2]$: $(enH_2)[Cd(HSeO_3)_2Br_2]$ (**1**), $(enH_2)[Cd(HSeO_3)_2Cl_2]$ (**2**), $(enH_2)[Co(HSeO_3)_2Br_2]$ (**3**), $(enH_2)[Co(HSeO_3)_2Cl_2]$ (**4**), $(enH_2)[Cu(HSeO_3)_2Br_2]$ (**5**), $(enH_2)[Cu(HSeO_3)_2Cl_2]$ (**6**), $(enH_2)[Mn(HSeO_3)_2Br_2]$ (**7**), $(enH_2)[Mn(HSeO_3)_2Cl_2]$ (**8**), $(enH_2)[Zn(HSeO_3)_2Br_2]$ (**9**), $(enH_2)[Zn(HSeO_3)_2Cl_2]$ (**10**), $(enH_2)[Ni(HSeO_3)_2Cl_2]$ (**11**).

	1	2	3	4	5	6	7	8	9	10	11
Radiation						MoKα, 0.71073					
Crystal system						monoclinic					
Space group						$P2_1/c$					
a (Å)	8.8222(4)	8.2957(5)	8.9395(6)	8.6750(4)	9.1833(4)	8.9953(3)	8.9465(4)	8.2958(3)	9.1862(4)	8.6699(4)	8.6420(8)
b (Å)	7.6140(3)	7.8094(3)	7.3147(4)	7.3277(3)	7.1548(3)	7.1677(2)	7.4460(3)	7.6712(2)	7.1516(2)	7.3448(2)	7.3081(4)
c (Å)	10.2481(5)	9.9433(5)	9.7558(8)	9.6812(4)	9.4845(5)	9.3819(4)	10.0240(5)	9.5977(4)	9.4849(4)	9.6996(4)	9.6000(9)
β (°)	114.196(6)	112.430(6)	111.904(9)	113.093(6)	110.608(5)	111.215(4)	112.720(6)	111.293(4)	110.624(4)	113.228(5)	112.999(11)
Volume (Å^3)	627.91(6)	595.44(6)	591.88(8)	566.10(4)	583.30(5)	563.91(3)	615.94(5)	569.09(3)	583.19(4)	567.59(4)	558.11(8)
D_{calc} (g/cm^3)	3.122	2.726	3.012	2.628	3.083	2.665	2.829	2.590	3.094	2.658	2.664
θ range (°)	3.45–33.64	3.41–33.26	3.58–38.06	3.60–35.53	3.66–33.49	3.68–35.65	3.51–33.72	3.50–35.49	3.66–35.66	3.59–35.42	3.68–27.99
h, k, l ranges	12→−12 11→−9 15→−14	12→−12 8→−12 14→−13	15→−15 11→−12 15→−16	−9→13 −9→11 −15→14	−13→12 −10→10 −12→12	−14→13 −11→11 −15→15	−13→12 10→−8 14→−13	−13→11 −10→12 −13→15	−14→14 −11→11 −14→15	−11→14 −11→7 −15→14	11→−11 9→−9 12→−12
Total reflections collected	2119	2019	4713	2319	1992	2395	2091	2362	2414	2339	1349
Unique reflections (R_{int})	1885 (0.032)	1702 (0.031)	3061 (0.08)	2009 (0.043)	1710 (0.054)	2101 (0.059)	1791 (0.035)	2109 (0.031)	2128 (0.042)	2089 (0.041)	1048 (0.075)
$R1[F > 4\sigma F]$, $wR1[F > 4\sigma F]$	0.023 (0.051)	0.025 (0.053)	0.047 (0.084)	0.029 (0.056)	0.035 (0.070)	0.024 (0.057)	0.030 (0.073)	0.022 (0.049)	0.028 (0.062)	0.028 (0.058)	0.039 (0.076)
Rall, wRall	0.028 (0.052)	0.033 (0.054)	0.082 (0.092)	0.036 (0.058)	0.043 (0.073)	0.030 (0.058)	0.037 (0.075)	0.026 (0.050)	0.035 (0.063)	0.033 (0.059)	0.058 (0.081)
Goodness of fit	1.053	0.984	0.989	1.056	1.095	1.026	1.107	0.981	1.125	1.047	1.058
CCDC number	2,271,293	2,271,295	2,271,296	2,271,297	2,271,298	2,271,307	2,271,300	2,271,301	2,271,306	2,271,305	2,271,304

Table 2. Geometrical parameters of MO_4X_2 polyhedra in $(enH_2)[M(HSeO_3)_2X_2]$.

Polyhedron	CdO$_4$Br$_2$	CdO$_4$Cl$_2$	CoO$_4$Cl$_2$	CuO$_4$Br$_2$	CuO$_4$Cl$_2$	MnO$_4$Br$_2$	MnO$_4$Cl$_2$	ZnO$_4$Br$_2$	ZnO$_4$Cl$_2$	NiO$_4$Cl$_2$
Bond valence for M^{2+}	2.04	2.08	2.00	1.89	2.09	2.11	2.04	2.09	1.90	2.01
Average bond length, Å	2.4387	2.3950	2.2243	2.2807	2.2329	2.3587	2.3032	2.2806	2.2318	2.1973
Polyhedral volume, Å^3	19.063	18.177	14.453	15.083	14.271	17.124	16.131	15.081	14.611	13.9603
Distortion index (bond length)	0.0768	0.0546	0.0884	0.1686	0.1532	0.1086	0.0735	0.1689	0.0866	0.08296

The largest anisotropy in the bond lengths is observed among the Cu and Zn compounds. The difference between the apical and equatorial bonds in [CuO_4Br_2] is as much as 0.871Å (distortion index = 0.168). In the most symmetrical [CdO_4Cl_2] octahedron, this difference drops to 0.293 Å (distortion index = 0.055). The strong distortion of the Cu and Zn polyhedral can be explained considering the low CFSE values and the Jahn–Teller effect (first order for the former and second order for the latter). Another reason for the distortion of the MO_4X_2 octahedra is extrinsic and caused by hydrogen bonds, both to oxygen and halogen vertices, from the $(enH_2)^{2+}$ or $(pipH_2)^{2+}$ templates, where the size of halogen also matters. The volumes of the MO_4X_2 octahedra vary from 14.27 Å^3 (CuO_4Cl_2) to 19.06 Å^3 (CdO_4Br_2). The M-X bond distances agree well with the reported values, e.g., Cd-Br distances of 2.7198(3) Å are only slightly shorter than those in the $CdBr_6$ octahedra in $CdBr_2$ (2.785(4)Å); the same applies to the Cd–Cl bond distances in $(enH_2)[Cd(HSeO_3)_2Cl_2]$ (2.5910(7) Å) and $CdCl_2$ (2.637(4)Å). Selenium forms the expected SeO_3 ψ-tetrahedron with two shorter (1.67–1.69Å) and one longer (1.75–1.77 Å) bond to the OH group (Figure 2) as expected for the $HSeO_3^-$ anion.

A typical crystal structure of the $(enH_2)[M(HSeO_3)_2X_2]$ (M = Cd, Co, Cu, Mn, Zn, Ni; X = Cl, Br) is shown in Figure 3a,b. The M^{2+} cations reside in centers of MO_4X_2 octahedra formed by the non-protonated oxygen atoms of the four $HSeO_3^-$ anions; these are very similar to those in the corresponding chloride compound (2.2881(17) and 2.3082(18) Å, respectively [21]). Each of the protonated nitrogen atoms of the enH_2^{2+} cation forms hydrogen bonds: two to the bromide anion and one to the oxygen atoms of two $HSeO_3^-$ species (Figure 3c). The halide anions hydrogen bonds are weakest (3.196(5)–3.435(3)Å). Therefore, the enH_2^{2+} cation forms the maximal number (6) of possible hydrogen bonds. Very similar environments are also observed in the compounds of manganese, cobalt, nickel, copper, and zinc.
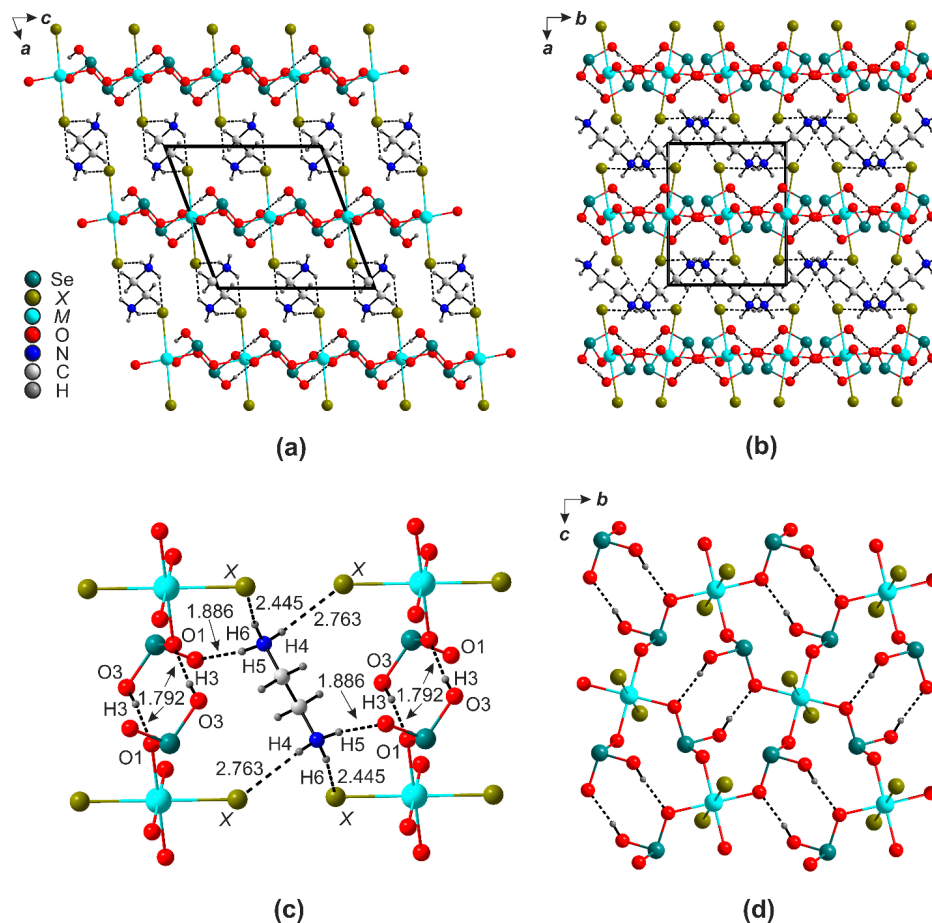

(a)　　　　　　　　　　　　　　　　　　**(b)**

(c)　　　　　　　　　　　　　　　　　　**(d)**

Figure 3. Projection of the structures of $(enH_2)[M(HSeO_3)_2X_2]$ onto *ac* (**a**) and *ab* (**b**) planes. Hydrogen

bonding systems: enH$_2$-*X*-enH$_2$ (**c**) and HSeO$_3$-HSeO$_3$ (**d**).

The [*MO$_4$X$_2$*] octahedra are stitched by the hydrogen-bonded (HSeO$_3^-$)$_2$ pairs into the [*M*(HSeO$_3$)$_2$*X$_2$*]$^{2-}$ layers (Figure 3d). In the structures of (enH$_2$)[*M*(HSeO$_3$)$_2$*X$_2$*], the O3-H1···O1 bond lengths (Table S1) change within 2.616(2)–2.653(4) Å, while the angles change within 158.11–175.90°. The enH$_2^{2+}$-HSeO$_3^-$ hydrogen bonds are rather insensitive to the nature of *M^{2+}* cations (2.798(2)–2.971(1)Å).

2.2. The (pipH$_2$)[Cd(HSeO$_3$)$_2$X$_2$] (X = Cl, Br) Series

In proper agreement with [21], two isostructural (pipH$_2$)[Cd(HSeO$_3$)$_2$*X$_2$*] compounds were prepared (Table 3).

In the structures of (pipH$_2$)[Cd(HSeO$_3$)$_2$*X$_2$*], the Cd atoms also center the [CdO$_4$X$_2$] octahedra (Figure 4a). The mean Cd-O separations in the [CdO$_4$Br$_2$] (2.335(3) Å) and [CdO$_4$Cl$_2$] (2.293(4) Å) in (enH$_2$)[*M*(HSeO$_3$)$_2$X$_2$] and (pipH$_2$)[Cd(HSeO$_3$)$_2$X$_2$] are rather close, yet Cd-*X* (<Cd-Br> = 2.653 Å, <Cd-Cl> = 2.587 Å).
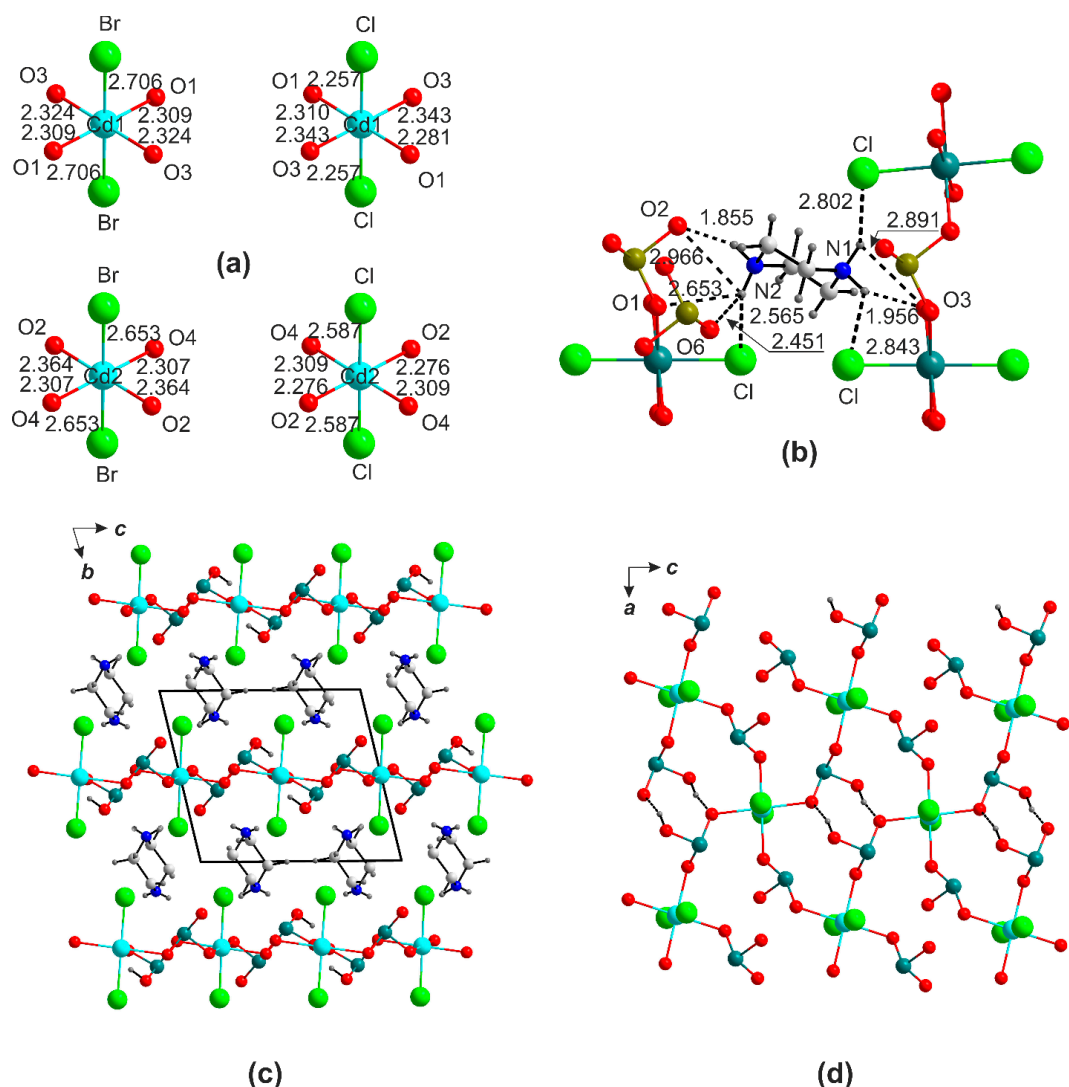
Figure 4. Cation coordination in the crystal structure of (pipH$_2$)[Cd(HSeO$_3$)$_2$*X$_2$*] (**a**). Hydrogen bonding systems: pipH$_2$-Br (**b**). Projection of the structures of (pipH$_2$)[Cd(HSeO$_3$)$_2$*X$_2$*] onto *ab* plane (**c**). The [Cd(HSeO$_3$)$_2$*X$_2$*]$^{2-}$ layer in the structure of (pipH$_2$)[Cd(HSeO$_3$)$_2$*X$_2$*] (**d**).

Table 3. Crystallographic and refinement parameters for (pipH₂)[Cd(HSeO₃)₂Cl₂] (**12**), (pipH₂)[Cd(HSeO₃)₂Br₂] (**13**), (pipH₂)[Co(HSeO₃)(Se₂O₅)]₂ (**14**), (pipH₂)[Mn(HSeO₃)(Se₂O₅)]₂ (**15**), (enH₂)(H₂SeO₃)Br₂ (**16**), (pipH₂)(ZnCl₄)(H₂O) (**17**), (mpipH₂)ZnCl₄(H₂O) (**18**), (enH₂)(NO₃)₂ 2H₂SeO₃ (**19**), (pipH₂)[Cd(HSeO₃)₂Cl₂](H₂O)₂ (**20**), (pipH₂)(NO₃)₂·2H₂SeO₃ (**21**).

	12	**13**	**14**	**15**	**16**	**17**	**18**	**19**	**20**	**21**
Radiation	MoK$_\alpha$, 0.71073									
Crystal system	triclinic				monoclinic				triclinic	monoclinic
Space group	P-1				$P2_1$/c			$P2_1$/c	P-1	$P2_1$/n
a (Å)/α (°)	7.6207(3)/ 77.077(4)	7.7373(2)/ 76.646(3)	7.4411(3)/ 114.766(4)	7.5632(3)/ 115.300(4)	8.0012(5)	6.5391(2)	14.2117(3)	5.9386(3)	7.14040(10)/ 107.419(2)	5.61000(10)
b (Å)/β (°)	9.4337(4)/ 88.138(4)	9.4999(3)/ 88.778(2)	8.5623(4)/ 93.329(3)	8.7844(3)/ 92.985(3)	11.1514(7)/ 90.012(5)	12.6400(3)/ 92.567(2)	12.6651(3)/ 102.492(2)	5.2221(3)/ 90.669(4)	7.5642(2)/ 95.832(2)	6.8184(2)/ 98.024(2)
c (Å)/γ (°)	10.0207(4)/ 68.552(4)	10.1340(3)/ 68.472(3)	9.2460(4)/ 114.568(4)	9.4451(3)/ 114.829(4)	6.8168(4)	13.8009(4)	13.6203(3)	21.0732(11)	9.0469(2)/ 106.206(2)	18.7159(5)
Volume (Å³)/Z	652.57(5)	672.53(4)	466.85(4)	493.96(4)	608.23(6)	1139.56(6)	2393.52(9)	653.48(6)	438.464(18)	708.90(3)
Dcalc (g/cm³)		3.043	3.331	3.068	2.620	3.053	2.906	2.257	2.828	2.202
θ range (°)		3.38–27.50	3.43–33.64	3.38–33.49	3.50–35.66	3.37–35.65	3.49–35.44	3.43–33.60	3.47–38.02	3.68–38.09
h, k, l ranges		10→-10 12→-12 13→-13	11→-10 12→-13 13→-13	10→-11 13→-13 14→-13	12→-10 15→-17 6→-10	10→-10 13→-20 20→-22	21→-22 20→-18 22→-20	7→-8 7→-7 27→-32	12→-12 12→-12 15→-14	9→-8 11→-10 31→-27
Total reflections collected		3084	3120	3331	2335	4741	4979	2234	4484	3622
Unique reflections (Rint)		2748 (0.057)	2624 (0.031)	2724 (0.042)	1887 (0.036)	4069 (0.035)	4379 (0.025)	1827 (0.06)	3997 (0.034)	3046 (0.037)
R1[$F > 4\sigma F$], wR1[$F > 4\sigma F$]		0.035 (0.085)	0.025 (0.045)	0.038 (0.087)	0.033 (0.076)	0.025 (0.049)	0.019 (0.042)	0.053 (0.14)	0.025 (0.56)	0.028 (0.62)
Rall, wRall		0.040 (0.087)	0.033 (0.046)	0.049 (0.089)	0.045 (0.079)	0.033 (0.051)	0.024 (0.043)	0.064 (0.15)	0.030 (0.57)	0.038 (0.65)
Goodness-of-fit		1.024	1.030	1.150	1.004	1.055	1.056	1.081	1.026	1.029
CCDC number	*	2,275,315	2,275,344	2,275,377	2,275,047	2,275,306	2,275,269	2,275,256	2,275,336	2,275,366

* only unit-cell parameters are given.

The bond differences in the CdO_4X_2 octahedra (0.318 and 0.577 Å for $[CdO_4Br_2]$ and $[CdO_4Cl_2]$, respectively) are smaller in $(pipH_2)[Cd(HSeO_3)_2X_2]$ compared to $(enH_2)[Cd(HSeO_3)_2X_2]$. The piperazinium cations form five hydrogen bonds of varying strength exclusive to the oxygen atoms of the $HSeO_3^-$ anions (Figure 4b), which are better recipients than the halides. The $[Cd(HSeO_3)_2X_2]^{2-}$ layers in the en and pip structures are nearly the same (Figure 4c,d). As the quality of the $(pipH_2)[Cd(HSeO_3)_2Cl_2]$ crystals was relatively low, several attempts were made to produce better ones.

In a single case, a crystal with quite different metrics was picked, which was found to belong to a new compound $(pipH_2)[Cd(HSeO_3)_2Cl_2]\cdot 2H_2O$ (Table 3) with a related composition but a totally different structure (Figure 5).In this case, two symmetry-independent Cd^{2+} cations reside in *trans*-CdO_2Cl_4 octahedra (Figure 5a) which share common Cl···Cl edges to form chains (Figure 5b). The $HSeO_3^-$ anions do not form pairs; they act as hydrogen bond acceptors from the $pipH_2^{2+}$ cations (Figure 5c). The $[CdCl_2(HSeO_3)_2]^{2-}$ chains are also involved in hydrogen bonding with water molecules.

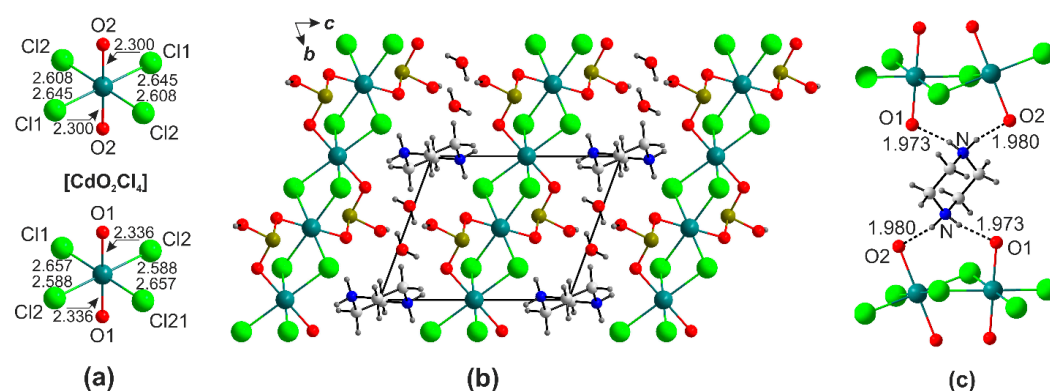**Figure 5.** The crystal structure of $(pipH_2)[Cd(HSeO_3)_2Cl_2]\cdot 2H_2O$. Cation coordination in the crystal structure of $(pipH_2)[Cd(HSeO_3)_2Cl_2]\cdot 2H_2O$ (**a**). Projection of the structure of $(pipH_2)[Cd(HSeO_3)_2Cl_2]\cdot 2H_2O$ onto the *bc* plane (**b**). Fragment of the structure with hydrogen bonds shown (**c**).

2.3. Halide-Free Framework Structures

The organic templates also contribute to formation of halide-free complex selenite diselenites of the $(diamineH_2)[M(HSeO_3)(Se_2O_5)]_2$ (M = Cd, Co, Mn, Zn) family (Table 3). These frameworks have been reported earlier for $(NH_3(CH_2)_4NH_3)[M(HSeO_3)(Se_2O_5)]_2$ (M = Zn, Co or Ni) series templated by tetramethylenediammonium cations [24]; these frameworks also seem to be rather elastic and readily incorporate cyclic piperazinium cations.

The newcomer to this family is Mn^{2+}. Overall, combinations of (protonated) SeO_3^{2-} and $Se_2O_5^{2-}$ are rather common in inorganic frameworks based on various *s-*, *d-*, and *f-* metals [25–30]. Their templating by various organic species is very likely to result in a variety of complex and elegant architectures. In the meantime, such species were not observed with the branched $mpipH_2^{2+}$ cation. A likely reason for this is the same as in the previous case: either the branched structure or the shape of the organic moiety.

In the $(pipH_2)[M(HSeO_3)(Se_2O_5)]_2$ (M = Co, Mn), the divalent cations center nearly regular MO_6 octahedra (Figure 6a), with a mean distance of 2.1039(18) and 2.181(4) Å, respectively. Three symmetry-independent Se atoms contribute to the $Se1Se2O_5^{2-}$ and $HSe3O_3^-$ anions (Figure 6b). The latter associate into chains aligned along a via. The $Se1O_3$ and $Se2O_3$ polyhedra share vertices with the MO_6 octahedra to form layers aligned in parallel (Figure 6c). Overall, a porous framework is formed (Figure 6d) with cavities filled by the piperazinium cations. The latter are for hydrogen bonds to the oxygen atoms of the framework. The channel size, estimated as the distance between the opposite oxygen atoms, is 4.13 × 5.58 Å.
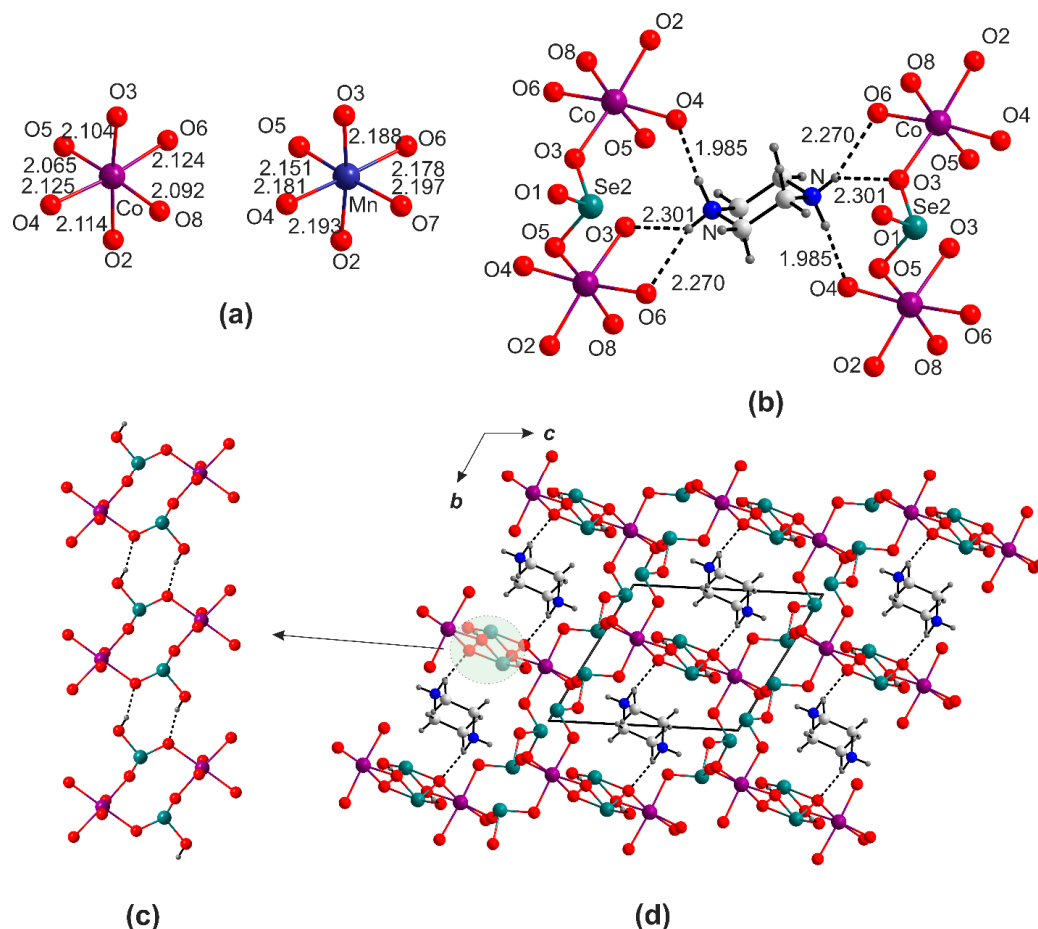
Figure 6. Cation coordination in the crystal structure of (pipH$_2$)[M(HSeO$_3$)(Se$_2$O$_5$)]$_2$ (**a**). Hydrogen bonding systems (**b,c**). Projection of the structures of (pipH$_2$)[M(HSeO$_3$)(Se$_2$O$_5$)]$_2$ onto the *bc* plane (**d**).

2.4. Ion-Molecular Crystals and Halometallates

Our previous studies have demonstrated that careful inspection of various crystals formed in selenite-containing systems may lead to discovery of unusual architectures, including first representatives of new intriguing families [31–34]. Therefore, all good quality crystals, including colorless (i.e., those evidently not containing Mn^{2+}, Co^{2+}, Ni^{2+}, or Cu^{2+}), were studied (Table 3). Formation of diammonium polyhalometallates was detected in many halide-containing runs, as illustrated by (pipH$_2$)ZnCl$_4$·H$_2$O [35,36], (mpipH$_2$)ZnCl$_4$·H$_2$O, non-centrosymmetric (pipH$_2$)[ZnBr$_4$], and (enH$_2$)[Cd$_2$Br$_6$(H$_2$O)], which contain both tetrahedrally and octahedrally coordinated cadmium [37]. The presence of excess acid (selenious of trifluoroacetic) liberates some free hydrohalic acid, which probably contributes to formation of these side products. In the structure of (pipH$_2$)[ZnCl$_4$](H$_2$O) (Figure 7a), Zn^{2+} centers a [ZnCl$_4$]$^{2-}$ tetrahedron (<Zn-Cl> = 2.2763 Å) connected to pip by hydrogen bonds (Figure 7b). The Cl atoms accept two hydrogen bonds (2.856(4) and 2.375(2) Å) from the pipH$_2^{2+}$ cation, and one from the water molecule (2.566(3) Å). A close chemical composition was also found for the tetrachlorozincate of mpip (Figure 7c,d); however, due to the different size and shape of the cation, as well as the lower number of hydrogen bonds (three for mpipH$_2^{2+}$ vs. four for pipH$_2^{2+}$), the structure is also different (Figure 7e,f). The mpipH$_2^{2+}$ cation has three "active" nitrogen-bound hydrogens, which form two single hydrogen bonds and one bifurcated hydrogen bond accepted by Cl- from two different [ZnCl$_4$]$^{2-}$ anions and one water molecule. The hydrogen atoms of the latter also form bonds to the chlorozincate anions.

The metal-free structure of (enH$_2$)X$_2$·2H$_2$SeO$_3$ (X = Cl and Br) (Figure 8) is the first "organic analog" of the *AX·n*H$_2$SeO$_3$ compounds (*A* is an alkali cation) [33,34], wherein the Se atom is also coordinated to three oxygen atoms, two of which are protonated to

form the H_2SeO_3 molecule (Figure 8a). In the structure of halides (take *X* = Br for example), these species and the enH_2^{2+} cations, as well as Br^-, link via hydrogen bonding to form a framework wherein the organic and inorganic parts form sublayers distantly reminiscent of the $AX \cdot nH_2SeO_3$ [33,34] (Figure 8a–c). The H_2SeO_3 molecules also form hydrogen bonds between each other (Figure 8d).
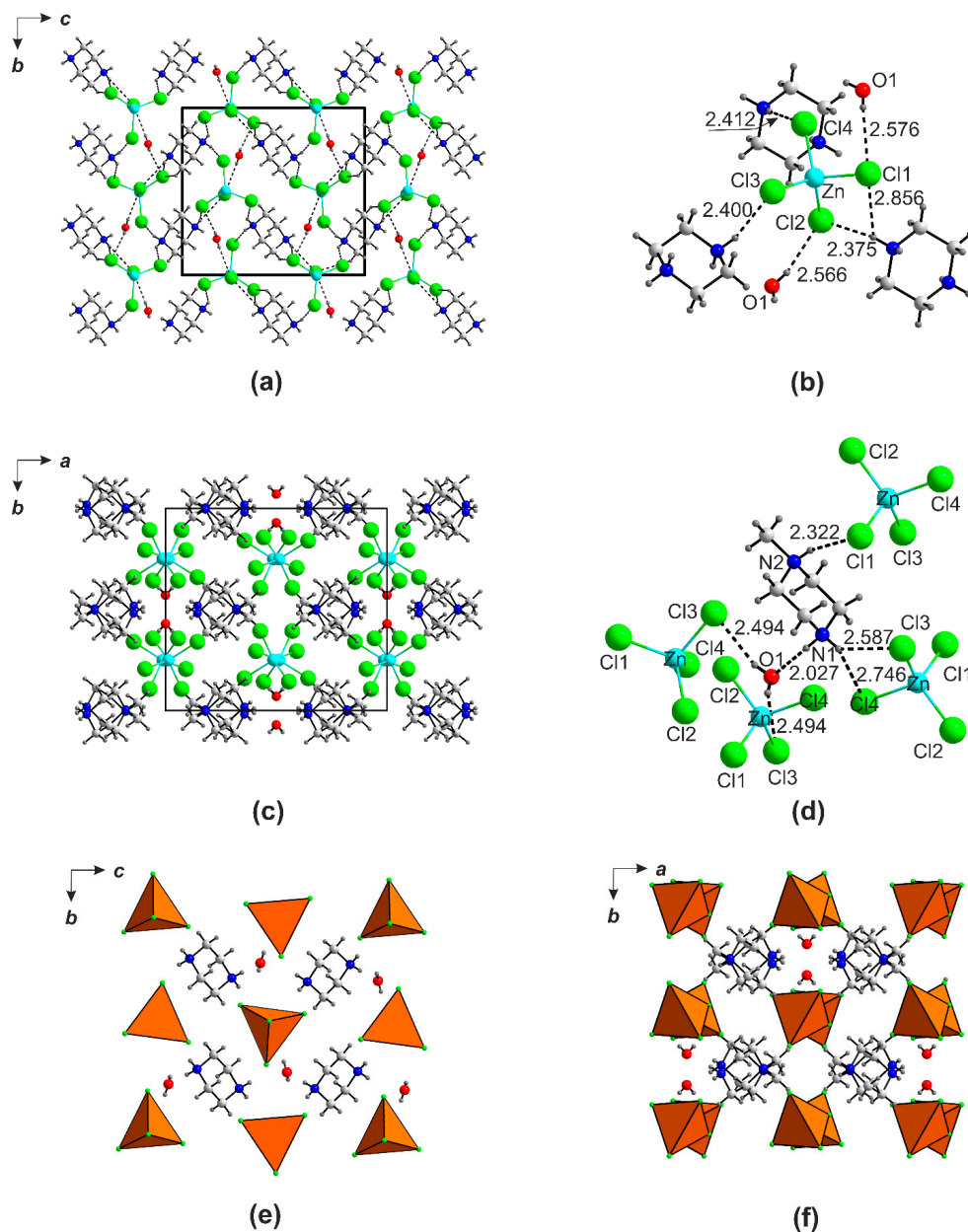

(a)

(b)

(c)

(d)

(e)

(f)

Figure 7. Projection of the structures of $(pipH_2)[ZnCl_4](H_2O)$ onto *bc* (**a**) and $(mpipH_2)ZnCl_4 \cdot H_2O$ onto *ab* (**c**) planes and hydrogen bonds system therein (**b**,**d**). Polyhedral representation of the crystal structure of $(pipH_2)[ZnCl_4](H_2O)$ onto the *cb* plane (**e**) and $(mpipH_2)ZnCl_4 \cdot H_2O$ (**f**) onto the *ab* plane (**f**).

The nitrate derivatives, $(enH_2)(NO_3)_2 \cdot 2H_2SeO_3$ and $(pipH_2)(NO_3)_2 \cdot 2H_2SeO_3$, have close chemical compositions but also different crystal structures (Figure 9). In the former structure (Figure 9a,c), the H_2SeO_3 species form chains aligned along *b*. They are decorated by the nitrate groups attached via hydrogen bonds to form ribbons. The enH_2^{2+} cations are situated between these. As in the previous case, both architectures can be considered to be pseudo-layered, yet with a different topology; the layers are formed by changed and neutral moieties. Both organic species form hydrogen bonds to oxygens of both NO_3^- and H_2SeO_3 moieties (Figure 9b,d).
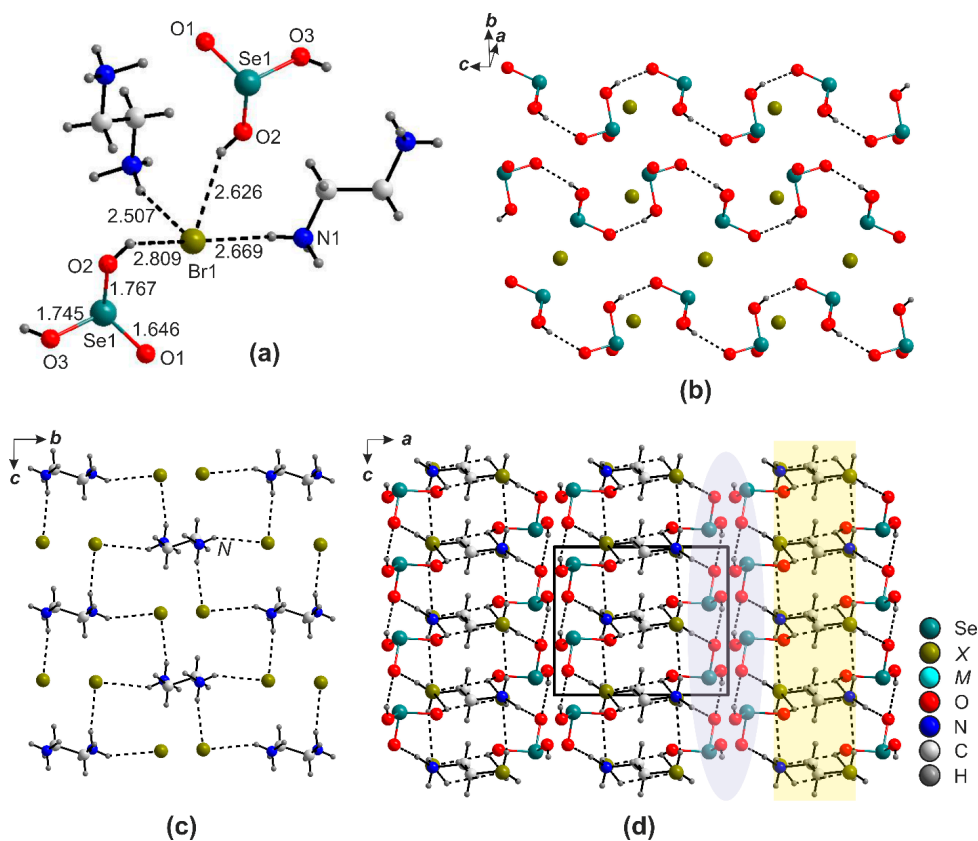
Figure 8. Hydrogen bonding in the structures of enH$_2$X$_2$·2H$_2$SeO$_3$ (X = Cl and Br) (**a–c**). Projection of the structure onto the *ac* plane (**d**).
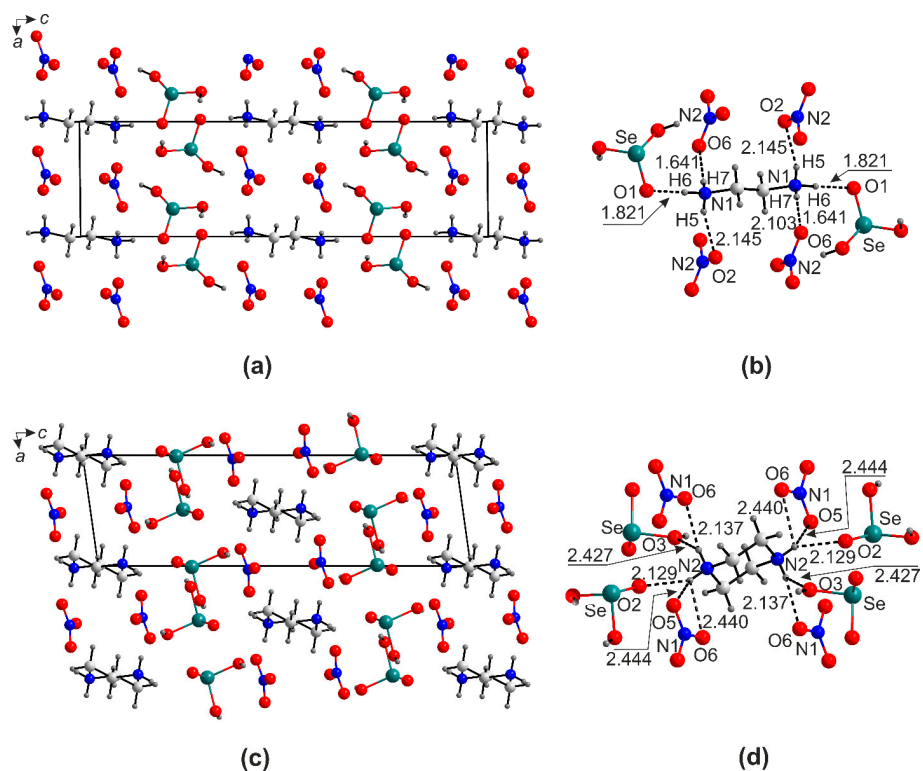
Figure 9. Projection of the structures of (enH$_2$)(NO$_3$)$_2$·2H$_2$SeO$_3$ onto the *ac* (**a**) plane. Hydrogen bonding in the structures of (enH$_2$)(NO$_3$)$_2$·2H$_2$SeO$_3$ (**b**). Projection of the structures of (pipH$_2$)(NO$_3$)$_2$(H$_2$SeO$_3$)$_2$ onto the *ac* (**c**) plane. Hydrogen bonding in the structures of (pipH$_2$)(NO$_3$)$_2$(H$_2$SeO$_3$)$_2$ (**d**).

2.5. Structural Trends in Organic Hydrogen Selenites

Table S1 contains 24 entries for hydrogen selenites containing organic cations. To determine the topology of mutual positioning of the organic and inorganic parts, we used the approach developed in [38]. For each structure, a diagram is constructed where green triangles designate the partially or fully protonated SeO_3 groups, with the OH vertices highlighted in brown, the organic species are shown as blue rectangles, and the water molecules are shown as red ovals. These structures can be divided into three groups: those containing only $HSeO_3^-$ (Figure 10), those also containing H_2SeO_3 molecules (Figure 11), and those containing crystal water molecules (Figure 12).
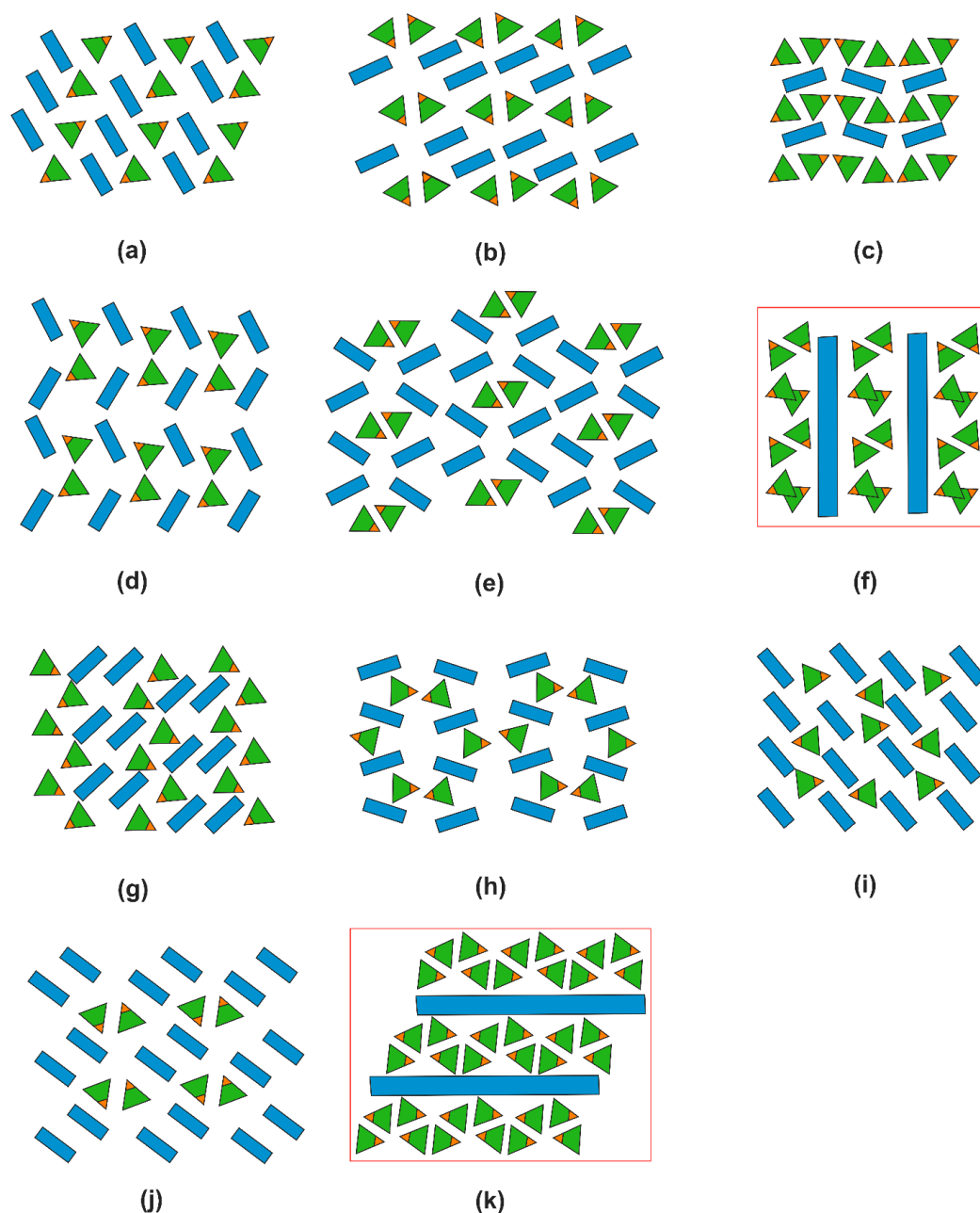

Figure 10. Diagrams for the organic hydrogen selenites $(BH)^+ \cdot HSeO_3^-$. The structures reported here are framed in red. $[C_2H_6NO_2][C_2H_5NO_2][HSeO_3]$ [39] (**a**), $[C_6H_{16}NO_3][HSeO_3]$ [40] (**b**), $[C_6H_{16}N_2][HSeO_3]$ [41] (**c**), $[C_4H_6N_3O][HSeO_3]$ [42] (**d**), $[C_9H_{12}NO_2][C_9H_{11}NO_2][HSeO_3]$ [43] (**e**), $(enH_2)(M(HSeO_3)_2X_2)$ (**f**), $[C_{11}H_{13}N_2O_2][HSeO_3]$ [44] (**g**), $[C_{13}H_{14}N_3][HSeO_3]H_2O$ [45] (**h**), $[C_8H_{20}N][HSeO_3]$ [46] (**i**), $[C_2H_7N_4O][HSeO_3]$ [47] (**j**), $(pipH_2)[Cd(HSeO_3)_2X_2]$ (**k**). The organic species are identified in Table S1.
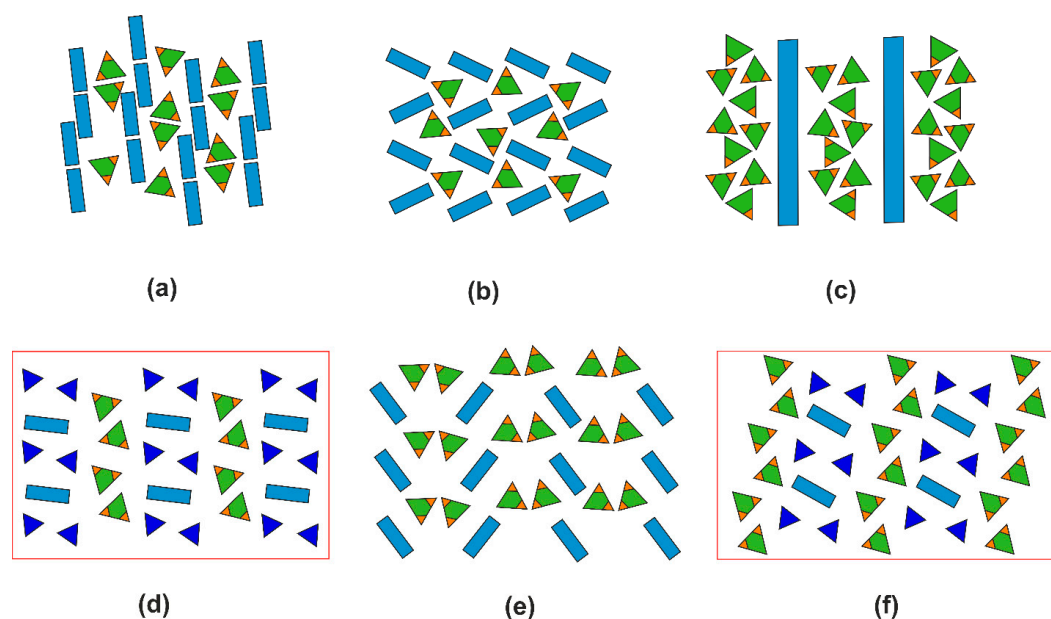
Figure 11. Diagrams for the structures containing organic matter and H_2SeO_3 molecules. As in the previous figure, the structures reported here are framed in red. $[C_2H_5NO_2][H_2SeO_3]$ [48] (**a**), $[C_5H_{11}NO_2][H_2SeO_3]$ [49] (**b**), $[C_{10}H_{16}N][HSeO_3][H_2SeO_3]$ [50] (**c**), $(enH_2)(NO_3)_2(H_2SeO_3)_2$ (**d**), $(enH_2)X_2(H_2SeO_3)_2$ (**e**), $(pipH_2)(NO_3)_2(H_2SeO_3)_2$ (**f**). The organic species are identified in Table S1.
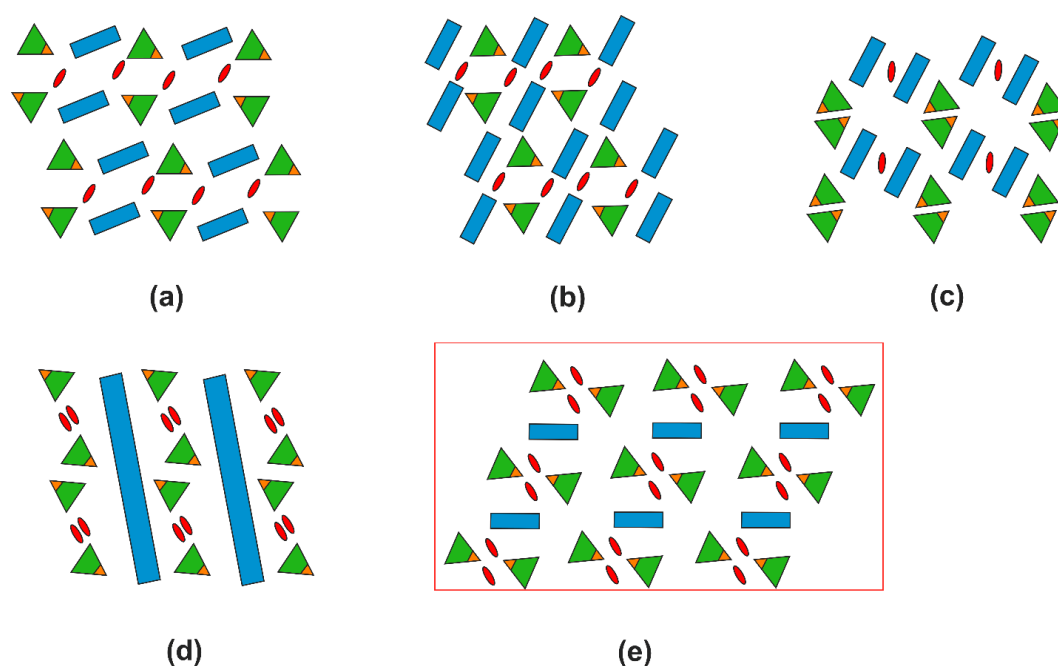
Figure 12. Diagrams for the structures containing extra water molecules: $[C_7H_8NO_2][HSeO_3]H_2O$ [51] (**a**), $[C_6H_8N][HSeO_3][H_2O]$ [52] (**b**), $[C_6H_{15}N_4O_2][HSeO_3]\cdot0.15H_2O$ [53] (**c**), and $[C_{36}H_{30}NP_2][HSeO_3][CH_2Cl_2][H_2O]$ [54] (**d**), $(pipH_2)[Cd(HSeO_3)_2Cl_2]\cdot2H_2O$ (**e**). The organic species are identified in Table S1.

In the structures of organic hydrogen selenites $(BH)^+\cdot HSeO_3^-$ (where *B* designates protonated organic matter), one can clearly distinguish the segregation of organic and inorganic species into layer-like areas, irrespective of the size and shape of the former. In the latter, the $HSeO_3^-$ species aggregate into dimers via hydrogen bonding. This trend is visible even in such complex structures as that of the phenylalanine and guanylurea derivatives, $[C_9H_{12}NO_2][C_9H_{11}NO_2][HSeO_3]$ and $[C_2H_7N_4O][HSeO_3]$, where the hydroselenite groups can be alternatively considered as being embedded into the organic sublattice.

The trend in segregation of the organic and inorganic matter can also be followed in the few structures containing neutral molecules of selenious acid (Figure 11). When both constituents are neutral (e.g., in co-crystals of amino acids), we can consider the result to be a hybrid organo-inorganic composite. A more complex pattern is observed for $(enH_2)(NO_3)_2 \cdot 2H_2SeO_3$ and $(pipH_2)(NO_3)_2 \cdot 2H_2SeO_3$, where there are several hydrogen bond donors and acceptors.

Addition of water molecules to these organo-inorganic architectures results in "delamination" into three types of layers; those formed by water molecules are either sandwiched between the organic matter layers or between those and the selenite groups (Figure 12). Note that the number of these entries is very small; no structure is known containing neutral molecules of both selenious acid and water.

Overall, the structures discussed here can be considered as complex organo-inorganic architectures. The segregation of the organic and inorganic parts can be understood considering that the former species aggregate due to the dominating Van der Waals (hydrophobic) interactions; they interact with the latter only via hydrogen bonding. The donors of "linking" hydrogen bonds are the protonated nitrogen atoms of the organic matter, while the recipients are the inorganic anions, including $HSeO_3^-$ and H_2SeO_3; the latter also interact via hydrogen bonding, but only between each other (Figure 3e), which is likely the cause of their aggregation. The size and shape of the organic molecules do not affect the type of hydrogen bonding.

2.6. Overall Remarks

The new compounds observed in our studies form several new families containing both known and new structure types, and their diversity and elegance is quite amazing. It is also evident that at least one half of these can be considered to be the first representatives of significantly more numerous groups. Due to almost unlimited diversity of organic hydrogen bond donors with both rigid and flexible backbones and, correspondingly, the topology of hydrogen bond directions, the structural chemistry of their derivatives also seems to be hardly restricted. However, some relationships can be traced and some new families predicted.

The most common structure, previously reported for $(enH_2)[M(HSeO_3)_2Cl_2]$ (M = Cd [21], Cu, and Co [19]) is observed for the majority of metal di-cations studied, including bromides and compounds of zinc. Three newcomers to this family are Mn^{2+}, Mg^{2+}, and Ni^{2+}, although the latter two only with some reluctance. The electronic structure of the metal di-cation is therefore not sufficient; the size of Mg^{2+} is relatively close to Zn^{2+} or Mn^{2+} [55]. We may tentatively assume, however, that because its electronic structure is different, the lack of d-orbitals hinders formation of Mg–X bonds even in the presence of a large excess of competing water molecules. Examples are quite abundant when, even in halide-rich media, products of ambient-temperature crystal hydrates mostly contain the initial $[Mg(H_2O)_6]^{2+}$ cations. Illustrative examples are provided by the structures of the $[Mg(H_2O)_6][ZnCl_4]$ and $[Mg(H_2O)_6]_2[MnCl_6]$ compounds [56,57], wherein Mg^{2+} and Zn^{2+} or Mn^{2+} are bonded selectively to the water molecules and chloride anions, respectively, as well as by synthetic analogs of carnallite [58]. The $[Ni(H_2O)_6]^{2+}$ cation present in the initial dilute solution does not undergo a Jahn–Teller distortion (high-spin d^8 configuration, $t_{2g}^6 e_g^2$) and is expected to be more inert (at least, under ambient conditions) towards ligand exchange compared to Mn^{2+} and Zn^{2+}, with CFSE = 0 and Co^{2+} and Cu^{2+} exhibiting an essential Jahn–Teller distortion. An illustration can be provided by the structures of $NiCd_2Cl_6 \cdot 12H_2O$ [59], which also contains isolated $[Ni(H_2O)_6]^{2+}$ octahedra in the cavities of a complex Cd^{2+}–Cl^-–H_2O framework, wherein Cd^{2+} easily adopts a mixed-ligand coordination. This may explain the absence of the corresponding $(enH_2)[M(HSeO_3)_2Br_2]$ species with M = Mg and Ni.

The non-rigid and relatively small ethylenediammonium cation, which forms as many as six hydrogen bonds, easily fits into the space between the hydroselenite-halide $[M(HSeO_3)_2X_2]^{2-}$ layers. With more voluminous and more rigid piperazinium, the layered

structure is observed only for Cu^{2+} (which is the commonest contributor to the layered hydroselenite family, vide supra) and the largest Cd^{2+}. Even then, the layered hydroselenite structure seems to lie on the stability edge, as exemplified by the formation of the structurally unrelated dihydrate. With smaller Mn^{2+}, Co^{2+}, or Zn^{2+}, only the "microporous" hydroselenite-diselenites are formed; Mg^{2+} also does not contribute to this family. This 3D framework is also relatively flexible and can host both linear-chain $(CH_2)_4(NH_3)_2^{2+}$ and piperazinium cations. Finally, the branched N-methylpiperazinium cation probably has no chance to contribute to any of these, and simpler and unconstrained structures of tetrahalometallates are formed instead; most starting solutions containing this cation produced no crystals at all. In targeted attempts to produce crystals of $(BH_2)(NO_3)_2 \cdot 2H_2SeO_3$ with B = pip and mpip, the formed solution produced the target crystals within several weeks, while the latter remained viscous. It should be noted, however, that nearly all solutions containing selenious acid become syrupy, and nearly glassy at the last stages of evaporation, which probably hinders crystallization.

The reluctance of most M^{2+} cations to coordinate NO_3^- in aqueous solutions can be expected given the high hygroscopicity of the respective nitrates (those of Mg and Mn deliquesce quite rapidly when exposed to air). It is also possible that cationic species with larger effective radii should be present, suggesting the ammonium "head" of the diamine comparable in size to NH_4^+ and K^+. We note that the former contributes to a relatively complex, strongly hydrogen-bonded $[(NH_4)_3(NO_3)][Cu(HSeO_3)_2(NO_3)_2]$ layered architecture [9], while the latter does not contribute at all [14]. It is possible that ammonium nitrate-related architectures can be produced using polyethylenepolyammonium species instead of discrete ammonium cations, e.g., $[(dienH_3)(NO_3)][Cu(HSeO_3)_2(NO_3)_2]$ or $[(trienH_4)(NO_3)_2][Cu(HSeO_3)_2(NO_3)_2]$ (dien = diethylenetriamine, trien = triethylenetetramine), etc.

The structures of the organic species containing both selenium and organics can thus be divided into three groups: (i) the "layered hydroselenites", containing all constituents, (ii) the halide-free "microporous structures", and (iii) the metal-free "ion-molecular crystals". For the first family, we predict the existence of new members with relatively flexible non-branched or short-branched backbones containing ammonium groups at the opposite ends which would fit the size of the $[M(HSeO_3)_2]$ grids, e.g., α,ω-polymethylenediammonium cations, $^+H_3N(CH_2)_nNH_3^+$. Note, however, that at least some of these can also contribute to the halide-free structures [26]. Formation of double Langmuir-like layers of alkylammonium cations, similar to $Cs_2[Co(HSeO_3)_2Cl_2]$ [17], is also possible. As the Cu- and Co-based compounds exhibit magnetic ordering [19], it may be of interest to see how the intralayer interactions would be affected by varying the interlayer distances by changing the spacer size. Some of these investigations are now in progress.

The second family of structures contains the $[M_2(HSeO_3)_2(Se_2O_5)_2]^{2-}$ frameworks with a limited inner space, so more voluminous species such as $mpipH_2^{2+}$ are probably too large to fit therein; the alternative found in our experiments is the formation of simpler structures of halometallates. Therefore, long chains of larger-cycle diamines (or polyamines) will most likely not be "admitted", including for compounds with branched backbones. Other topologies are known, however, e.g., based on vanadyl cations, where such species act as templates for chiral porous frameworks [60].

The third group, represented as yet by a pair of isostructural compounds, $enH_2X_2 \cdot 2H_2SeO_3$ (X = Cl and Br) and the non-analogous nitrate $enH_2(NO_3)_2 \cdot 2H_2SeO_3$, also promises to be diverse as the hydrogen-bonded nets of H_2SeO_3 molecules and are expected to be the very flexible and adaptable. Another example is $(pipH_2)(NO_3)_2 \cdot 2H_2SeO_3$. Due to the unlimited variability of the organic species, which need not necessarily be hydrogen bond donors or acceptors (similar to alkali cations), one can expect formation of various structures, including non-centrosymmetric structures, by careful choice of the corresponding templates. Formation of non-centrosymmetric organically templated inorganic selenites has been documented [8,60]; further perspectives in this direction are quite promising. Note that while nitrates and halides can contribute to similar structures when

these anions form purely ionic bonds to the cationic species (alkali cations), the analogies disappear when hydrogen bonding is enforced. The very symmetrical halide anions can form hydrogen bonds in all possible directions, while the rigid planar nitrate group has a fixed geometry of hydrogen bond acceptors.

The few structures of selenium-free halometallates observed in our work also fit very well into the structural trends observed in this relatively well-addressed family. The non-centrosymmetric structure of (pipH$_2$)[ZnBr$_4$] is a full analog of (pipH$_2$)[CoBr$_4$] [61] and (pipH$_2$)[CdI$_4$] [35]. The (pipH$_2$)[ZnCl$_4$](H$_2$O) is in turn isostructural to (pipH$_2$)[CdBr$_4$](H$_2$O) [62]; therefore, the structures and hydration state of compounds containing [ZnCl$_4$]$^{2-}$ and [ZnBr$_4$]$^{2-}$ (or [CoBr$_4$]$^{2-}$) are similar to those containing [CdBr$_4$]$^{2-}$ and [CdI$_4$]$^{2-}$ or [HgI$_4$]$^{2-}$, respectively, which points at the X^-/M^{2+} size ratio as the structure-driving factor. Hence, the (mpipH$_2$)[ZnCl$_4$](H$_2$O) is expected to be isostructural to the (mpipH$_2$)[CdBr$_4$](H$_2$O) reported in [63]; however, the latter was not structurally characterized. Thus, the family hosts at least four non-centrosymmetric and one complex layer structure. Its future also seems intriguing.

3. Materials and Methods

3.1. Synthesis

The starting compounds were the organic diamines, selenious acid, and corresponding metal halides or nitrates. Unimolar working solutions of all compounds were prepared first. Next, MX_2, H$_2$SeO$_3$, and diamine solutions were mixed together to provide a 1:1:3 molar ratio. Generally, 1 mL of MX_2 solution was mixed with 3 mL of 1M H$_2$SeO$_3$. Next, 1 mL of the diamine solutions was added dropwise upon stirring with a small glass bar. The 50% excess of the selenious acid was shown in [10,13,21] to be necessary to suppress formation of insoluble metal selenites and competitive formation of halometallates, which easily form if extra hydrohalic acid is added [13]. Commonly, precipitation or turbidity due to formation of MSeO$_3$·aq was observed after diamine was introduced, which mostly disappeared after stirring and heating to 50–60 °C for 5 to 10 min on a hotplate. Until clearance, several drops of water were added to keep the solution volume constant. With M = Cu or Cd, which form less soluble selenites, the flaky green and white (respectively) precipitates were dissolved after heating and adding 0.1 to 0.7 mL of trifluoroacetic acid in the case of halides and 0.1–0.5 mL of 50% nitric acid for nitrates, according to the protocols developed earlier [13,15]. (In one or two cases, traces of CdSeO$_3$·aq persisted but dissolved over time when crystals of the targeted compounds started to form.) The halide solutions (colorless in case of M^{II} = Mg, Zn and Cd, initially pink for Mn, violet for Co, green in the case of Ni, and blue in the case of Cu) were left to evaporate at ambient conditions. Crystallization started in a few weeks, after the color of halide-bearing solutions containing Co and Cu turned lilac (Co), green (Cu–Cl), or brownish (Cu–Br); the color of the Cu- and Co-containing crystals was bluish-green and dark violet, respectively. The intermediate change in solution colors likely indicates transient formation of [MX_4^{2-}] due to free hydrohalic acid present in solution. No color change was observed for the solutions containing Mn and Ni (as well as in all experiments with nitrates). The Mn- and Ni-bearing crystals were grayish-pink and brownish yellow. The crystals grown in Mg-containing solutions were of relatively low quality. Sometimes, small amounts of red selenium were precipitated due to reduction of selenious acid, which did not affect the formation and growth of the target crystals. The exception was dmeda, which was rapidly oxidized by selenious acid; this compound was therefore excluded from further studies. The crystals were collected and kept in closed vials under a drop of the mother liquor. Further evaporation of the mother liquors led to repeated deposition of crystals with similar color and appearance. The majority of these runs provided the target hydroselenite halides for en, just a few for pip, and none for mpip. In most cases, crystals of some side products were also observed, which were formed either due to the off-stoichiometric reagents ratio of the initial charge, or instead of the targeted compound. Based on the combination of diamine,

metal cation, and anion, these side products may contain either all constituents, or only some of these; those exhibiting new compositions and/or structures are discussed in detail.

A related pattern was observed for the nitrate solutions, except that the color of the crystals corresponded to those of the hydrated M^{2+} cations. The only exception was observed in the case of Mn^{2+}, which produced black needles of low quality; such a color change is indicative of oxidation of Mn^{2+} into Mn^{3+} or Mn^{4+}. This compound will be addressed elsewhere. In these cases, no target compound was observed; crystals of a new compound $(enH_2)(NO_3)_2 \cdot 2H_2SeO_3$ were produced with all runs with en. With pip and mpip, no crystalline produces were observed for the nitrate runs.

As in the previous studies, in the last stages the liquors commonly became dark and viscous, produced no more crystals, and were discarded. It is worth noting that crystals were the first to form with en, next with pip, and with greater difficulty in the case of mpip; some solutions containing mpip produced no crystals but only viscous residues.

According to the classification suggested above, the produced species were: (i) $(enH_2)[M(HSeO_3)_2X_2]$ (M = Cd, Co, Cu, Mn, Zn, Ni; X = Cl, Br) and $(pipH_2)[M(HSeO_3)_2X_2]$ (M = Cd, X = Cl and Br; M = Cu, X = Cl; (ii) $(pipH_2)[M(HSeO_3)(Se_2O_5)]_2$ (M = Mn, Co, Zn); (iii) $enH_2X_2 \cdot 2H_2SeO_3$ (X = Cl, Br, and NO_3) and $(pipH_2)(NO_3)_2 \cdot 2H_2SeO_3$; and (iv) $(pipH_2)[ZnCl_4](H_2O)$, $(mpipH_2)[ZnCl_4](H_2O)$, and $(pipH_2)[ZnBr_4]$. The side products most likely come from the off-stoichiometric ratio of the initial solutions; these were observed in most deposited samples. The three new compounds $enH_2X_2 \cdot 2H_2SeO_3$ (X = Cl, Br, and NO_3) were prepared in targeted runs by mixing the $1M$ working solutions of en, HX, and H_2SeO_3 taken in a 1:2.1:2 volume ratio; large (up to several mm) colorless crystals were produced after several weeks of evaporation at ambient conditions.

3.2. Single Crystal X-ray Study

The collected crystals were taken out of the mother liquors, attached to glass fibers, and transferred to a Rigaku XtaLAB Synergy-S diffractometer (Tokyo, Japan) equipped with a PhotonJet-S detector (Tokyo, Japan) operating with MoKα radiation at 50 kV and 1 mA. A single crystal was chosen and more than a hemisphere of data was collected with a frame width of 0.5° in ω, and 5–15 s was spent counting for each frame. The data were integrated and corrected for absorption applying a multiscan type model using the Rigaku Oxford Diffraction programs CrysAlis Pro (Rigaku OD, 2015) (Tokyo, Japan). The experiments were performed at 150 K. The unit cell parameters were calculated by the least-squares method. The structures were solved by direct methods using WinGX version 2020.1 (Glasgow, UK) [64] and Olex2 version 1.3.0 (Regensburg, Germany) [65] software. The final solutions include the coordinates and anisotropic thermal parameters of atoms except for hydrogens. Hydrogen atoms were located using the mathematical part of the Olex2 program.

Experimental data for the $(enH_2)[M(HSeO_3)_2X_2]$ series are collected in Table 1 (except M = Mg, where the crystals were of low quality). All these compounds are isostructural; some trends are discussed below. The corresponding data for the piperazinium compounds are listed in Table 3. In contrast to the alkali-bearing family, in no case did we observe formation of organic-containing layered hydroselenite nitrates; the organic and inorganic matter crystallized separately yielded $MSeO_3 \cdot aq$ (or $M(HSeO_3)_2$); and with en and pip, new compounds $(BH_2)(NO_3)_2 \cdot 2H_2SeO_3$ were observed, which are considered below. The simplest side results are also discussed here, while some others with $3D$ structures will be reported in separate contributions.

References

1. Ok, K.M. Toward the rational design of novel noncentrosymmetric materials: Factors influencing the framework structures. *Acc. Chem. Res.* **2016**, *49*, 2774–2785. https://doi.org/10.1021/acs.accounts.6b00452.

2. Lin, H.; Li, Y.Y.; Li, M.Y.; Ma, Z.; Wu, L.M.; Wu, X.T.; Zhu, Q.L. Centric-to-acentric structure transformation induced by a stereochemically active lone pair: A new insight for design of IR nonlinear optical materials. *J. Mater. Chem. C* **2019**, *7*, 4638–4643. https://doi.org/10.1039/C9TC00647H.

3. Handy, J.V.; Zaheer, W.; Rothfuss, A.R.M.; McGranahan, C.R.; Agbeworfi, G.; Andrews, J.L.; García-Pedraza, K.E.; Ponis, J.D.; Ayala, J.R.; Ding, Y.; et al. Lone but not alone: Precise positioning of lone pairs for the design of photocatalytic architectures. *Chem. Mater.* **2022**, *34*, 1439–1458. https://doi.org/10.1021/acs.chemmater.1c03762.

4. Hu, C.L.; Mao, J.G. Recent advances on second-order NLO materials based on metal iodates. *Coord. Chem. Rev.* **2015**, *288*, 1–17. https://doi.org/10.1016/j.ccr.2015.01.005.

5. Yan, M.; Xue, H.G.; Guo, S.P. Recent achievements in lone-pair cation-based infrared second-order nonlinear optical materials. *Cryst. Growth Des.* **2021**, *21*, 698–720. https://doi.org/10.1021/acs.cgd.0c01407.

6. Millet, P.; Johnson, M.; Pashchenko, V.; Ksari, Y.; Stepanov, A.; Mila, F. New copper(II)–lone electron pair elements–oxyhalides compounds: Syntheses, crystal structures, and magnetic properties. *Solid State Ion.* **2001**, *141–142*, 559–565. https://doi.org/10.1016/S0167-2738(01)00765-2.

7. Kim, S.H.; Yeon, J.; Sefat, A.S.; Mandrus, D.G.; Halasyamani, P.S. Stereo-active lone-pair control on the ferromagnetic behavior in $VO(SeO_2OH)_2$: A new acentric ferromagnetic material. *Chem. Mater.* **2010**, *22*, 6665–6672. https://doi.org/10.1021/cm102659w.

8. Charkin, D.O.; Grishaev, V.Y.; Omelchenko, T.A.; Nazarchuk, E.V.; Stefanovich, S.Y.; Siidra, O.I. $KNO_3 \cdot 3H_2SeO_3$ and $NaHSeO_3 \cdot 3H_2SeO_3$: Two non-centrosymmetric co-crystals. *Solid State Sci.* **2023**, *137*, 107116. https://doi.org/10.1016/j.solidstatesciences.2023.107116.

9. Lafront, A.M.; Trombe, J.C. Layered hydrogenselenite I. Synthesis, structure redetermination of $Cu(HSeO_3)_2(H_2O)_2$ and determination of $Cu(HSeO_3)_2(NO_3)_2^{2-} \cdot 2NH_4^+ \cdot NH_4NO_3$. Structural relationships of these complexes with $Cu(HSeO_3)_2$. *Inorg. Chim. Acta* **1995**, *234*, 19–25. https://doi.org/10.1016/0020-1693(95)04500-9.

10. Lafront, A.M.; Trombe, J.C.; Bonvoisin, J. Layered hydrogenselenites II. Synthesis, structure studies and magnetic properties of a novel series of bimetallic hydrogenselenites: $Cu(HSeO_3)_2 \cdot MCl_2(H_2O)_4$, M(II) = Mn, Co, Ni, Cu, Zn. *Inorg. Chim. Acta* **1995**, *238*, 15–22. https://doi.org/10.1016/0020-1693(95)04659-W.

11. Trombe, J.C.; Lafront, A.M.; Bonvoisin, J. Synthesis, structure and magnetic measurement of a new layered copper hydrogenselenite: $Cu(HSeO_3)_2 \cdot NH_4Cl$. *Inorg. Chim. Acta* **1997**, *262*, 47–51. https://doi.org/10.1016/S0020-1693(97)05501-1.

12. Kovrugin, V.M.; Krivovichev, S.V.; Mentré, O; Colmont, M. $[NaCl][Cu(HSeO_3)_2]$, NaCl-intercalated $Cu(HSeO_3)_2$: Synthesis, crystal structure and comparison with related compounds. *Z. Krist.–Cryst. Mat.* **2015**, *230*, 573–577. https://doi.org/10.1515/zkri-2015-1849.

13. Charkin, D.O.; Grishaev, V.Y.; Markovski, M.R.; Nekrasova, D.O.; Siidra, O.I. Influence of the alkali cation size on the Cu^{2+} coordination environments in $(AX)[Cu(HSeO_3)_2]$ (A = Na, K, NH_4, Rb, Cs; X = Cl, Br) layered copper hydrogen selenite halides. *Z. Krist.–Cryst. Mat.* **2019**, *234*, 739–747. https://doi.org/10.1515/zkri-2019-0042.

14. Markovski, M.R.; Charkin, D.O.; Nekrasova, D.O.; Siidra, O.I. Novel layered copper hydrogen selenite nitrates: Synthesis, structure, and spectroscopic properties. *Z. Krist.–Cryst. Mat.* **2019**, *234*, 749–756. https://doi.org/10.1515/zkri-2019-0036.

15. Grishaev, V.Y.; Siidra, O.I.; Markovski, M.R.; Charkin, D.O.; Omelchenko, T.A.; Nazarchuk, E.V. Synthesis and crystal structure of two novel polymorphs of $(NaCl)[Cu(HSeO_3)_2]$: A further contribution to the family of layered copper hydrogen selenites. *Z. Krist.–Cryst. Mater.* **2023**, *238*, 177–185. https://doi.org/10.1515/zkri-2023-0004.

16. Spirovski, F.; Wagener, M.; Stefov, V.; Engelen, B. Crystal structures of rubidium zinc bis(hydrogenselenate(IV)) chloride $RbZn(HSeO_3)_2Cl$, and rubidium zinc bis(hydrogenselenate(IV)) bromide $RbZn(HSeO_3)_2Br$. *Z. Krist.-New Cryst. Struct.* **2007**, *222*, 91–92. https://doi.org/10.1524/ncrs.2007.0037.

17. Wagener, M. Synthese, Charakterisierung Und Struktur-Chemische Aspekte Von Kupfer- Und Silberchalkogenohalogeniden Sowie Von Halogeno- Und Oxochalkogenaten(IV). Ph.D. Thesis, Uinversität Siegen, Siegen, Germany, 2005. Available online: https://d-nb.info/97663936X/34 (accessed on 15 May 2023).

18. Harrison, W.T.A.; Johnston, M.G. Syntheses and structures of two selenite chloride hydrates: $Co(HSeO_3)Cl \cdot 3H_2O$ and $Cu(HSeO_3)Cl \cdot 2H_2O$. *Z. Anorg. Allg. Chem.* **2000**, *626*, 2487–2490. https://doi.org/10.1002/(SICI)1521-3749(200004)626:4<867::AID-ZAAC867>3.0.CO;2-7.

19. Feng, M.-L.; Prosvirin, A.V.; Mao, J.G.; Dunbar, K.R. Syntheses, structural studies, and magnetic properties of divalent Cu and Co selenites with organic constituents. *Chem. Eur. J.* **2006**, *12*, 8312–8323. https://doi.org/10.1002/chem.200600031.

20. Johnston, M.G.; Harrison, W.T.A. Cobalt hydrogen selenite chloride dihydrate, $Co(HSeO_3)Cl\ 2H_2O$. *Acta Crystallogr. E* **2003**, *59*, i62–i64 https://doi.org/10.1107/S1600536803006378.

21. Pasha, I.; Choudhury, A.; Rao, C.N.R. An organically templated open-framework cadmium selenite. *Solid State Sci.* **2003**, *5*, 257–262. https://doi.org/10.1016/S1293-2558(02)00100-0.

22. Effenberger, H. $Cu(SeO_2OH)_2$: Synthesis and crystal structure. *Z. Krist.* **1985**, *173*, 267–272. https://doi.org/10.1524/zkri.1985.173.3-4.267.

23. Momma, K.; Izumi, F. VESTA 3 for three-dimensional visualization of crystal, volumetric and morphology data. *J. Appl. Crystallogr.* **2011**, *44*, 1272–1276. https://doi.org/10.1107/S0021889811038970.

24. Udayakumar, D.; Rao, C.N.R. Organically templated three-dimensional open-framework metal selenites with a diamondoid network. *J. Mater Chem.* **2003**, *13*, 1635–1638. https://doi.org/10.1039/B303323F.

25. Koskenlinna, M.; Valkonen, J. The crystal structure of $PrH_3(SeO_3)_2(Se_2O_5)$, a compound with selenite and diselenite groups. *Acta Chem. Scand.* **1977**, *31a*, 457–460. https://doi.org/10.3891/acta.chem.scand.31a-0457.

26. Koskenlinna, M.; Valkonen, J. Crystal structure of manganese(III) hydrogen selenite diselenite, $MnH(SeO_3)(Se_2O_5)$. *Acta Chem. Scand.* **1977**, *31a*, 638–640. https://doi.org/10.3891/acta.chem.scand.31a-0638.

27. Rao, C.N.R.; Behera, J.N.; Dan, M. Organically-templated metal sulfates, selenites and selenates. *Chem. Soc. Rev.* **2006**, *35*, 375–387. https://doi.org/10.1039/b510396g.

28. Wickleder, M.S. $Sm_2Se_5O_{13}$: A selenite–diselenite according to $Sm_2(SeO_3)(Se_2O_5)_2$. *Z. Anorg. Allg. Chem.* **2006**, *632*, 2377–2379. https://doi.org/10.1002/zaac.200600172.

29. Jiang, H.-G.; Mao, J.-G. Syntheses, crystal structures and optical properties of the first strontium selenium(IV) and tellurium(IV) oxychlorides: $Sr_3(SeO_3)(Se_2O_5)Cl_2$ and $Sr_4(Te_3O_8)Cl_4$. *J. Solid State Chem.* **2008**, *181*, 345–354. https://doi.org/10.1016/j.jssc.2007.12.007.

30. Jones, P.G.; Schwartzmann, E.; Sheldrick, G.M.; Timpe, H. Preparation and crystal structure of di-gold(III)bis(selenite) diselenite, $Au_2(SeO_3)_2(Se_2O_5)$. *Z. Naturforsch.* **1981**, *36*, 1050–1052. https://doi.org/10.1515/znb-1981-0826.

31. Markovski, M.R.; Siidra, O.I.; Charkin, D.O.; Vladimirova, V.A.; Tsirlin, A.A.; Grishaev, V.Y. $Li_2(Se_2O_5)(H_2O)_{1.5} \cdot CuCl_2$, a salt-inclusion diselenite structurally based on tetranuclear Li_4 complexes. *Dalton Trans.* **2020**, *49*, 7790–7795. https://doi.org/10.1039/d0dt01260b.

32. Markovski, M.R.; Siidra, O.I.; Charkin, D.O.; Grishaev, V.Y. Layered calcium hydrogen selenite chlorides $Ca(HSeO_3)Cl$ and $Ca(HSeO_3)Cl(H_2O)$, the first halides obtained in the $CaCl_2$–SeO_2–H_2O system. *Z. Krist.–Cryst. Mat.* **2020**, *235*, 439–443. https://doi.org/10.1515/zkri-2020-0054.

33. Markovski, M.R.; Siidra, O.I.; Charkin, D.O.; Nazarchuk, E.V.; Grishaev, V.Y. Molecular inorganic polymers: Synthesis and crystal structures of $KCl \cdot 2H_2SeO_3$ and $CsCl \cdot H_2SeO_3$. *Z. Krist.–Cryst. Mat.* **2020**, *235*, 553–557. https://doi.org/10.1515/zkri-2020-0062.

34. Wang, H.; Liu, L.; Hu, Z.; Wang, J.; Zhu, M.; Meng, Y.; Xu, J. $RbCl \cdot (H_2SeO_3)_2$: A salt-inclusion selenite featuring short UV cut-off edge and large birefringence. *Inorg. Chem.* **2023**, *62*, 557–564. https://doi.org/10.1021/acs.inorgchem.2c03787.

35. Ishihara, H.; Hatano, N.; Horiuchi, K.; Terao, H. NQR Study of piperazinium tetrahalogenometalates(II) $[C_4H_{12}N_2]MX_4$ (M = Zn, Cd, Hg; X = Br, I). *Z. Naturforsch.* **2002**, *57*, 343–347. https://doi.org/10.1515/zna-2002-6-710.

36. Kefi, R.; Ben, N.C. Crystal structure of piperazinium tetrachlorozincate monohydrate, $(C_4H_{12}N_2)[ZnCl_4] \cdot H_2O$. *Z. Krist.–New Cryst. Struct.* **2005**, *220*, 241–242. https://doi.org/10.1524/ncrs.2005.220.14.251.

37. Krishnan, V.G.; Dou, S.Q.; Paulus, H.; Weiss, A. Solid phases from the liquid system $H_2N(CH_2)_2NH_2$–$CdBr_2$–HBr–H_2O. An X-ray and $^{79,81}Br$–NQR study of $(H_3N(CH_2)_2NH_3)CdBr_4$, $(H_3N(CH_2)_2NH_3)(CdBr_3)_2 \cdot H_2O$, and $(H_3N(CH_2)_2NH_3)_2CdBr_6$. *Ber. Bunsenges. Phys. Chem.* **1991**, *95*, 1256–1264. https://doi.org/10.1002/bbpc.19910951015.

38. Krivovichev, S.V. *Structural Crystallography of Inorganic Oxysalts*; Oxford University Press: Oxford, UK, 2009; 320p.

39. Nemec, I.; Cisarova, I.; Micka, Z. Study of the family of glycine–selenious acid addition compounds: Crystal structure of diglycine hydrogen selenite and vibrational spectra and DSC measurement of diglycine hydrogen selenite and monoglycine–selenious acid crystals. *J. Solid State Chem.* **1998**, *140*, 71–82. https://doi.org/10.1006/jssc.1998.7854.

40. Lukevics, E.; Arsenyan, P.; Shestakova, I.; Domracheva, I.; Kanepe, I.; Belyakov, S.; Popelis, J.; Pudova, O. Cycloaddition reactions of nitrile oxides to silyl- and germyl-substituted thiophene-1,1-dioxides. *Organometallics* **2002**, *18*, 3187–3193. https://doi.org/10.1021/om9902129.

41. Nemec, I.; Chudoba, V.; Havlicek, D.; Cisarova, I.; Micka, Z. Preparation, crystal structure, vibrational spectra, and thermal behavior of N,N′-dimethylpiperazinium(2+) hydrogen selenite. *J. Solid State Chem.* **2001**, *161*, 312–318. https://doi.org/10.1006/jssc.2001.9317.

42. Takouachet, R.; Benali-Cherif, R.; Benali-Cherif, N. Cytosinium hydrogen selenite. *Acta Crystallogr.* **2014**, *E70*, o186–o187. https://doi.org/10.1107/S1600536814001275.

43. Gharzaryan, V.V.; Fleck, M.; Petrosyan, A.M. New salts of amino acids with dimeric cations. *Proc. SPIE Int. Conf. Laser Phys.* **2010**, *7998*, 107–115. https://doi.org/10.1117/12.890269.short?SSO=1.

44. Paixao, J.A.; Silva, M.R.; Beja, A.M.; Eusebio, E. Crystal structure and properties of L-tryptophanium hydrogen selenite. *Polyhedron* **2006**, *25*, 2021–2025. https://doi.org/10.1016/j.poly.2005.12.028.

45. Paixao, J.A.; Matos Beja, A.; Ramos Silva, M.; de Matos Gomes, E.; Martin-Gil, J.; Martin-Gil, F.J. *N,N* -diphenylguanidinium hydrogenselenite monohydrate. *Acta Crystallogr.* **1997**, *C53*, 1113–1115. https://doi.org/10.1107/S0108270197004472.

46. Wang, J.-J.; Tessier, C.; Holm, R.H. Analogue reaction systems of selenate reductase. *Inorg. Chem.* **2006**, *45*, 2979–2988. https://doi.org/10.1021/ic0521630.

47. Ritchie, L.K.; Harrison, W.T.A. 1-Carbamoylguanidinium hydrogenselenite. *Acta Crystallogr.* **2003**, *E59*, o1296–o1298. https://doi.org/10.1107/S1600536803017380.

48. Ondracek, J.; Walzelova, M.; Micka, Z.; Novotny, J. Structure of glycine-selenious acid (1/1). *Acta Crystallogr.* **1992**, *C48*, 391–392. https://doi.org/10.1107/S0108270191008235.

49. Paixao, J.A.; Matos Beja, A.; Ramos Silva, M.; Alte da Veiga, L.; Martin-Gil, J.; Martin-Gil, F.; de Matos Gomes, E. Crystal structure of betaine dihydrogen selenite, $C_5H_{13}NO_5Se$. *Z. Krist. New Cryst. Struct*. **1997**, *212*, 51–52. https://doi.org/10.1524/ncrs.1997.212.1.51.

50. De Matos Gomes, E.; Matos Beja, A.; Paixao, J.A.; de Veiga, L.A.; Ramos Silva, M.; Martin-Gil, J.; Martin-Gil, F.J. Synthesis, structure and thermal behavior of benzyltrimethylammonium trihydrogen selenite. *Z. Krist. Cryst. Mater.* **1995**, *210*, 929–933. https://doi.org/10.1524/zkri.1995.210.12.929.

51. Kamali, N.; OMalley, C.; Mahon, M.F.; Erxleben, A.; McArdle, P. The use of sublimation catalysis and polycrystalline powder templates for polymorph control of gas phase crystallization. *Cryst. Growth Des.* **2018**, *18*, 3510–3516. https://doi.org/10.1021/acs.cgd.8b00268.

52. Takouachet, R.; Benali-Cherif, R.; Bendeif, E.-E.; Benali-Cherif, N.; Pillet, S.; Schaniel, D. Structural analysis and IR-spectroscopy of a new anilinium hydrogenselenite hybrid compound: A subtle structural phase transition. *Inorg. Chim. Acta* **2016**, *446*, 6–12. https://doi.org/10.1016/j.ica.2016.02.047.

53. De Matos Gomes, E.; Nogueira, E.; Fernandes, I.; Belsley, M.; Paixao, J.A.; Matos Beja, A.; Ramos, S.M.; Martin-Gil, J.; Martin-Gil, F.; Mano, J.F. Synthesis, structure, thermal and non-linear optical properties of L-argininium hydrogen selenite. *Acta Crystallogr.* **2001**, *B57*, 828–832. https://doi.org/10.1107/S01087681010098880.

54. Canossa, S.; Graiff, C. Role of bis(triphenylphosphine)iminium cation $[PNP]^+$ on the crystal packing of $[PNP]^+[HSeO_3]^-$ solvate salt. *Crystals* **2018**, *8*, 151–155. https://doi.org/10.3390/cryst8040151.

55. Shannon, R.D. Revised effective ionic radii and systematic studies of interatomic distances in halides and chalcogenides. *Acta Crystallogr.* **1976**, *A32*, 751–767. https://doi.org/10.1107/S0567739476001551.

56. Duhlev, R.; Macicek, J. Structure of magnesium zinc tetrachloride hexahydrate $MgZnCl_4·6H_2O$. *Acta Crystallogr.* **1991**, *C47*, 1573–1575. https://doi.org/10.1107/S0108270191001798.

57. Waizumi, K.; Masuda, H.; Fukushima, N. Structural and energetic studies on double salts of $M(II)Mg_2Cl_6·12H_2O$ (M=Ca, Mn, Cd) by X-ray diffraction and density functional methods. *Inorganica Chim. Acta* **1995**, *238*, 121–127. https://doi.org/10.1016/0020-1693(95)04692-3.

58. Waizumi, K.; Masuda, H.; Ohtaki, H.; Scripkin, M.Y.; Burkov, K.A. Crystallographic investigations of $[Mg(H_2O)_6]XCl_3$ double salts (X^+ = K^+, Rb^+, Cs^+, NH_4^+): Crystal structure of $[Mg(H_2O)_6]CsCl_3$. *Am. Miner.* **1991**, *76*, 1884–1888.

59. Leclaire, A.; Borel, M.M. Structure de l hexachlorure de dicadmium et de nickel dodecahydrate. *Acta Crystallogr.* **1980**, *B36*, 3088–3090. https://doi.org/10.1107/S0567740880010850.

60. Olshansky, J.H.; Tran, T.T.; Hernandez, K.J.; Zeller, M.; Halasyamani, P.S.; Schrier, J.; Norquist, A.J. Role of hydrogen-bonding in the formation of polar achiral and nonpolar chiral vanadium selenite frameworks. *Inorg. Chem.* **2012**, *51*, 11040–11048. https://doi.org/10.1021/ic3015496.

61. Tlili, H.; Walha, S.; Elleuch, S.; Ali, B.F.; Naïli, H. Structural, vibrational, DFT and optical studies of a new non-centrosymmetric hybrid material $(C_4H_{12}N_2)[CoBr_4]$. *J. Mol. Struct.* **2018**, *1152*, 303–330. https://doi.org/10.1016/j.molstruc.2017.09.096.

62. Ishihara, H.; Horiuchi, K.; Gesing, T.M.; Dou, S.Q.; Buhl, J.C.; Erk, P. Crystal structures of piperazinium tetrabromocadmate(II)-monohydrate $[C_4H_{12}N_2]CdBr_4·H_2O$, piperazinium tetraiodocadmate(II) $[C_4H_{12}N_2]CdI_4$, and Bis(trimethylsulphonium) Tetrabromocadmate(II) $[(CH_3)_3S]_2CdBr_4$. *Z. Naturforsch.* **2002**, *57b*, 503–508. https://doi.org/10.1515/znb-2002-0505.

63. Battaglia, L.P.; Corradi, A.B.; Bruni, S.; Cariati, F.; Koman, M. Piperazinium and *N*-methyl-piperazinium tetrahalocadmates(II) containing discrete $[CdX_4]^{2-}$ units. *Inorg. Chim. Acta.* **1991**, *187*, 141–147. https://doi.org/10.1016/S0020-1693(00)90386-4.

64. Farrugia, L.J. WinGX suite for small-molecule single-crystal crystallography. *J. Appl. Crystallogr.* **1999**, *32*, 837–838.

65. Dolomanov, O.V.; Bourhis, L.J.; Gildea, R.J.; Howard, J.A.K.; Puschmann, H. OLEX2: A complete structure solution, refinement and analysis program. *J. Appl. Crystallogr.* **2009**, *42*, 339–341.

66. Chen, H.; Gao, W.; Zhu, M.; Gao, H.; Xue, J.; Li, Y. A highly selective OFF–ON fluorescent sensor for zinc in aqueous solution and living cells. *Chem. Commun.* **2010**, *46*, 8389–8391.

67. Krumbe, W.; Haussuhl, S. Structure and physical properties of orthorhombic guanidinium phthalate, $[CN_3H_6]_2C_8H_4O_4$, and guanidinium hydrogen L-aspartate, $[CN_3H_6]C_4H_6NO_4$. *Z. Kristallogr. Cryst. Mater.* **1987**, *179*, 267–279.

68. Lukevics, E.; Arsenyan, P.; Shestakova, I.; Domracheva, I.; Kanepe, I.; Belyakov, S.; Popelis, J.; Pudova, O. Synthesis, structure and cytotoxicity of organoammonium selenites. *Appl. Organomet. Chem.* **2002**, *16*, 228–234.